PAUL SCHERRER INSTITUT	Project EURISOL Design Study
Title: Design of the EURISOL converter target	Registration: TM-34-07-05
Author: K. Samec Co-Author:	Issued: 31.07.2007

Summary :

The design of a 4 MW liquid metal neutron spallation target featuring a cusp-shaped beam window is described in the present design study.

Starting from first principles and then working through simplified local models successive iterations to the design have been carried out to fulfil most if not all the requirements. The design is mostly driven by the 4 MW heat deposition, but also by the hydraulic stability and efficiency as well as the structural integrity, all within the constraints imposed by tight geometric and environmental considerations.

We acknowledge the financial support of the European Community under the FP6 “Research Infrastructure Action-Structuring the European Research Area” EURISOL DS Project contract no 515768 RIDS. The EC is not liable for the use that can be made of the information contained herein.

Verteiler

Abt.	Empfänger / Empfängerinnen	Expl.	Abt.	Emfpänger / Empfängerinnen	Expl.
CERN	Mats Lindroos	1			
	Jacques Lettry	1			
	Yacine Kadi	1			
PSI					
-NUM	Kurt Clausen	1			
-ASQ	Werner Wagner	1			
	Friedrich Groeschel	1			
	Karel Samec	1			
	Sergejs Dementjev	1			
-LTH	Brian Smith	1			
	Trevor Dury	1			
IPUL	J. Freibergs	1			
	E. Platacis	1			
	I. Platniecks	1			

	Expl.
Bibliothek	1
Reserve	
Total	14
Seiten	
Beilagen	
Informationsliste	
D 1 2 3 4 5 8 9 A	
Visum Abt.-/Laborleitung:	

R e v i s i o n L i s t

Chapter	**Issue**	**Author** **Date**	**Modification**
All	1	K. Samec 31-07-07	Original version

C o n t e n t s

-

List of Figures

List of Tables

-

List of Symbols

Parameters variables, and abbreviations:

a	[m/s]	Speed of sound
C_P	[J/kg/K]	Thermal capacity
CFD		Computational Fluid Dynamics
dpa		Displacement per atom
E_t	[N/mm^2]	Tensile elastic modulus
FEM		Finite Element Method
f	[Hz]	Frequency
h_f	[W/mK]	Heat transfer coefficient
G	[N/mm^2]	Shear elastic modulus
LM		Liquid Metal
N	[-]	Number of cycles
P	[Bar]	Pressure
RCCMR		French (CEA) standard design and construction rules for mechanical components of FBR nuclear islands
T	[°C]	Temperature
t	[sec.]	Time
U	[m/s]	Fluid average speed in tube
α	[1/K]	One-dimensional secant expansion coefficient
Δ	[-]	Difference, change
ϕ	[m^3/s],[l/s]	Flow rate
λ	[W/m/s]	Thermal conductivity
ν	[kg/m/s]	Dynamic viscosity
ν_{El}	[-]	Poisson coefficient relating tensile / shear modulus
ρ	[kg/m^3]	Density

R e f e r e n c e D o c u m e n t s

-

[Ref1] Best-estimate fit for EURISOL Heat Deposition Profiles
Memo_Power_Deposition K. Samec 24.01.07

[Ref2] Stress Analysis of the EURISOL DS converter target
TM-34-06-02 Q. Pretet et al. 02.10.2006 / Issue3

[Ref3] Thermo hydraulic optimisation of the EURISOL DS converter target
TM-34-06-04 M. Ashrafi-Nik et al 15.12.2006 / Issue 2

[Ref4] Declared Material List for MEGAPIE
MPS-QA-GF34-002/5 F. Gröschel

[Ref5] Baseline parameters Eurisol-DS task #2 “Multi-MW target station
02-25-2006-0011 Y. Kadi 11/09/2006

1 Introduction

The design of the converter target is a key element of the Eurisol project. It draws on existing know-how at PSI in relation to the design and operation of liquid-metal based neutron spallation sources such as the Megapie initiative and the ESS project. The former has actually been in operation for a full 4 months in late 2006, the latter has been studied at length over a number of years.

Compared to existing designs and in particular Megapie which had been designed for 1 MW, one of the mains challenges of the Eurisol target is to operate safely at power levels of up to 4 MW.

In the Eurisol concept, the converter target is surrounded by fissions targets which can generate interesting rare isotopes when the fission material (UC or similar) inside the fission targets is hit by neutrons leaving the liquid metal converter target where the neutrons are produced by spallation.

A high neutron flux is therefore required to improve the yield in the fission targets. This goal may be achieved by injecting a high power proton beam into the liquid metal converter target.

2 Scope

The present document describes the latest stage in the design of the Eurisol converter target (August 2007) and explains the guiding principles behind the current design.

The converter target described hereafter is to be tested in a full-scale hydraulic test. Therefore, the current document also describes instrumentation which is needed for a hydraulic test but may be left out in a production unit.

Constraints pertaining to an isotope production unit, notably irradiation and the proton beam heat deposition are taken into account in the current design so that the design for the hydraulic test may be used in a production facility later on if it is proven succesful in the hydraulic test. A thorough analysis of the design is therefore presented which covers all aspects relevant to operational conditions.

Manufacturing aspects are also covered so as to demonstrate the current design is realistic. Most of the structure is made from commercial-grade stainless steel which is readily available and can be easily processed.

3 Design environment

The device must be designed within the parameters set out in Ref [5], in particular relating to;

- The power and shape of the proton beam
- The flow rate and entrance/exit temperature of the liquid metal (still open)
- The outer dimensions of the target
- The interface requirements and connections for instrumentation (still open)
- The dose level
- The lifetime of the target

3.1 Definition of the proton beam

The proton beam is defined in [Ref1] for two different sizes of beams; a sigma of 15mm and a sigma of 25mm. The reference contains also an analytical function which approximates the heat deposition calculated from the neutronic calculation of Monte-Carlo simulations. A comparison of the deposition according to depth, both in the approximation and the Monte Carlo output is shown in Figure 3-1 below.

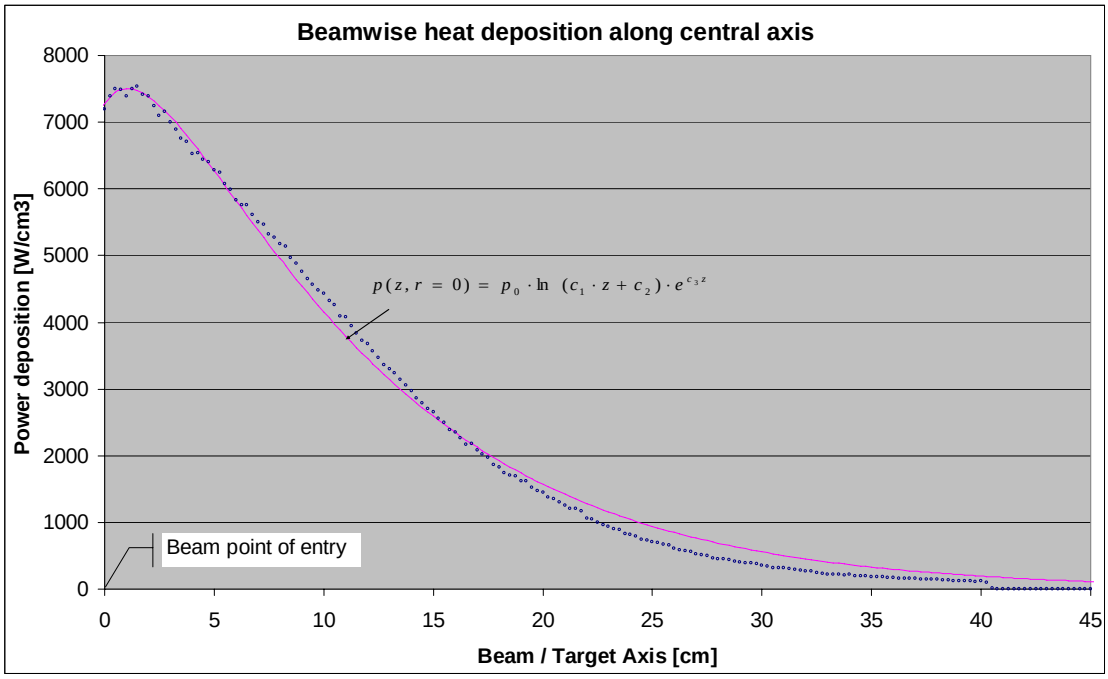

Figure 3-1. Power deposition in converter target

3.2 Hydraulic constraints

The Liquid Metal (LM) loop comprises a pump, a heat exchanger, filters, isotope extraction stations, sump tanks and assorted equipment, all of which operate within certain boundaries. Fundamental design criteria for the loop need therefore been set out at systems level, some of which may be found in Ref [5]. Most importantly the need to limit the LM temperature imposes constraints on the liquid metal flowing through the target, as set out in the table below.

Parameter	symbol	value	unit
Liquid compound	Hg	13.5	kg/l
Flow rate	ϕ	172	kg/s
Entrance temperature	T_{in}	< 60	C
Exit temperature	T_{out}	< 180	C
		> 150	
Pressure drop	ΔP	< 5	Bar
Static pressure	P_0	< 5	Bar

Table 1: Operational constraints on the liquid metal target from Ref [5]

3.3 Constraints from reference design requirements

The Eurisol isotope production unit is built in such a way to allow a cylinder-shaped converter target to be inserted in its centre. Figure 3-2 below gives an overview of the concept defined by Y. Kadi in Ref[5] and revised in later work.

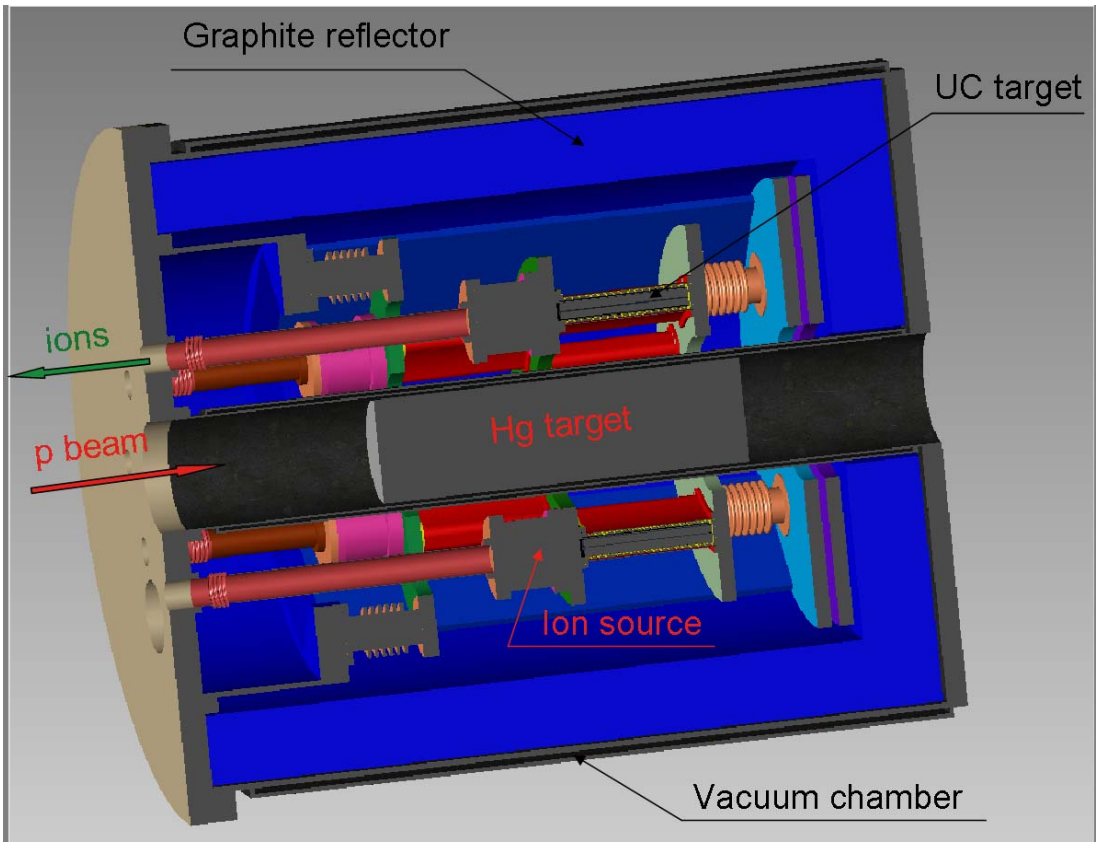

Figure 3-2. Eurisol Concept of the converter target surrounded by fission boxes and ion sources.

Such a concept allows only limited space for the converter target since the Uranium Carbide (UC) fission boxes have to be placed as close to the converter for maximum fission efficiency to be attained. The diameter retained for the converter target should therefore not exceed 150 [mm], in particular in the area located directly in line with the UC fission boxes.

3.4 Dose level, beam trips and operational lifetime

The number of beam trips and the dose level are critical to establishing with some degree of certainty the operational lifetime of the converter target, in particular the most exposed part, i.e. the proton beam window.

As these parameters are not yet firmly established, and in view of the uncertainty surrounding the fatigue properties of T91 steel under conditions of high irradiation it seems prudent to design a converter target capable of withstanding irradiation damage and ultimate failure of the window. It is therefore necessary to adopt a strategy for mitigating the eventual consequences of a liquid metal leak (such as the containment strategy in Megapie) as well as allowing for rapid and complete drainage of the converter target and subsequent exchange of the window, the part most likely to fail.

3.5 Material properties

T91 Martensite steel is selected for the converter a target, as it is a well-proven alloy for conventional nuclear applications and has been used on the lower target container in Megapie where it was subjected to heavy proton bombardment during 4 months at close to 1 MW beam power. The reasons for the choice are good radiation resistance and elevated temperature performance. Corresponding material values are extracted from [Ref4].

The choice of liquid is limited to mercury; as explained in the previous section, LBE and lead have not been retained by project management.

3.5.1 Properties of T91

Allowable design stress

The allowable stress documented in the French RCCMR standards **are applicable to irradiation levels below 2 [dpa]**, a dose the window is guaranteed to exceed after a number of weeks. Hence the values in the table below are used as a best estimate for design purposes, but as mentioned in section 3.5 provisions for dealing with a leak and exchanging the window should be planned in at an early stage.

T	°C	20	50	100	150	200	250	300	350	400	450	500	550	600
σ	N / mm^2	193	193	193	193	192	190	187	183	174	163	146	126	101

Table 2: Allowable design stress for T91 Martensite steel, temperature dependency

Linear thermal expansion coefficient

The temperature dependency for the thermal expansion coefficient is as follows

T	ºC	20	100	200	300	400	500	600	700
α_m	10^{-6}/K	10.4	10.8	11.2	11.6	11.9	12.2	12.5	12.7
α_i	10^{-6}/K	10.4	11.1	11.9	12.4	13.0	13.6	13.8	

Table 3: Linear thermal expansion coefficient for T91 Martensite steel, temperature dependency

Where: α_m *mean coefficient between 20ºC and T*
α_i *instantaneous coefficient at T*

Young`s Modulus

The temperature dependency for the stiffness modulus follows is as follows

E [MPa] = 207300 – 64.58 T for 20ºC < T < 500ºC

E [MPa] = 295000 – 240 T for 500ºC < T < 600ºC

T	ºC	20	100	200	300	400	500	600	700
E	[MPa]	206000	199500	194400	187900	181500	175000	151000	127000

Table 4: Young's modulus for T91 Martensite steel, temperature dependency

Poisson Coefficient

The coefficient ν is 0.3 for all temperatures.

The shear modulus G [MPa] is calculated according to G = E/2(1+ν).

Density

The density of T91 steel as a function of temperature is described in the table below.

T	ºC	20	100	200	300	400	500	600
ρ	kg/m^3	7730	7710	7680	7650	7610	7580	7540

Table 5: Density for T91 Martensite steel, temperature dependency

Thermal capacity

The thermal capacity of T91 steel as a function of temperature is described in the table below.

T	ºC	20	50	100	150	200	300	400	500	600
Cp	J/kg/K	448.85	462.76	484.11	503.92	523.04	562.69	609.96	671.75	754.96

Table 6: Thermal capacity for T91 Martensite steel, temperature dependency

Conductivity

The thermal conductivity of T91 steel as a function of temperature is described in the table below.

T	ºC	20	100	200	300	400	500	600
λ	W / m	25.9	27.0	28.1	28.8	29.2	29.0	28.5

Table 7: Thermal conductivity for T91 Martensite steel, temperature dependency

3.5.2 Properties of Mercury

Mercury properties are fairly constant with temperature below the boiling point which is heavily pressure dependent. Variations of physical properties are mostly small for the temperature range of interest (60-200C). In order to achieve the highest possible safety margin against boiling, pressurised mercury is used, for which the properties are listed below.

T Cp	Pr -	Cp J/kg/K	ν Kg/m/s	λ W / m	ρ kg/m3
20	0.0249	139.6	1.55E-03	8.69	13579
50	0.0207		1.40E-03	9.4	13506
100	0.0162	137.3	1.24E-03	10.51	13384
150	0.0134		1.13E-03	11.49	13264
200	0.0116	135.9	1.05E-03	12.34	13145
300		135.4			12880
350					12760
450		136.3			
456	Boiling point at 5 Bar				

Table 8: Mercury liquid metal properties at 5 Bar

4 Design description.

4.1 Design iteration process.

Successive design iterations have been fully documented in [Ref2] and [Ref3], which were aimed at reaching the following goals;

- Largest possible margin against boiling in LM at 5 Bar static pressure (456 C)
- Smallest possible pressure loss in LM.
- Smallest possible cavitation risk in the back-flow areas of the target.
- No large unstable structures in the LM, particularly where the proton beam is deposited.
- Stresses in the structure lower than the allowable RCCMR design values.

In order to achieve so many objectives, different design options were examined and their effect calculated with CFD for hydraulic and thermal aspects and FEM for the thermo-mechanical stresses. The overall concept of the target is shown in schematic form in the cross-section below.

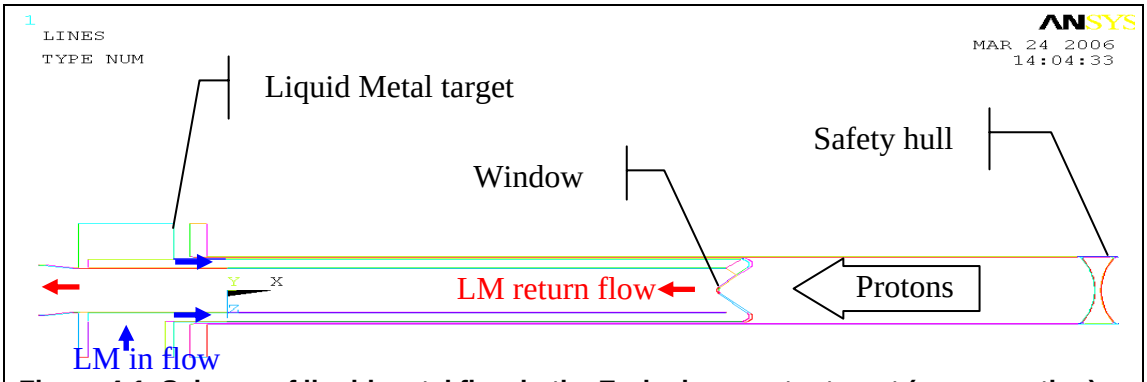

Figure 4-1. Scheme of liquid metal flow in the Eurisol converter target (cross-section)

The design possibilities for achieving these goals were examined in the successive iterations and comprise the following options;

- Narrowing the channel before the window to accelerate the flow locally.
- Holes through the guide tube to feed fresh LM from the entrance channel into the back-flow.
- Increasing the thickness of the guide tube to reduce the section of the back-flow and accelerate the fluid after which is hit by the proton beam.
- Guide vanes over the window to accelerate the fluid locally were the proton beam hits the target.
- Additional guide vanes at the forward end of the guide tube to help the flow turn back and reduce pressure losses and cavitation risk.
- Guide vanes in the back-flow to break up turbulence.

- Reducing the thickness of the window where the proton beam enters to facilitate extraction of the heat deposited. Increasing the thickness outside the footprint of the beam to enhance resistance to internal pressure.

The effect of each change was assessed in relation to the original design, which comprised a cusp-shaped window and a plain cylindrical 2mm thick guide tube design as shown in Figure 4-1. Each new feature is then either adopted or rejected, based on the goals outlined above. A successful feature is retained and becomes an integral part of the new design base from which further changes are attempted. The detail of these iterations is omitted in this document but can be consulted in [Ref2] and [Ref3]. The next sections describe in full the characteristics of the final design.

4.2 Design description

The optimised design for the mock-up (and if the hydraulic test is successful the final converter target) features a variable thickness guide tube for accelerating the liquid metal out of the spallation zone and a series of vanes at the forward end to both reverse the flow at minimum pressure loss and also to accelerate the liquid metal over the window so as to enhance cooling at the point of entry of the proton beam. The overall configuration is shown in Figure 4-2 and Figure 4-3 hereafter.

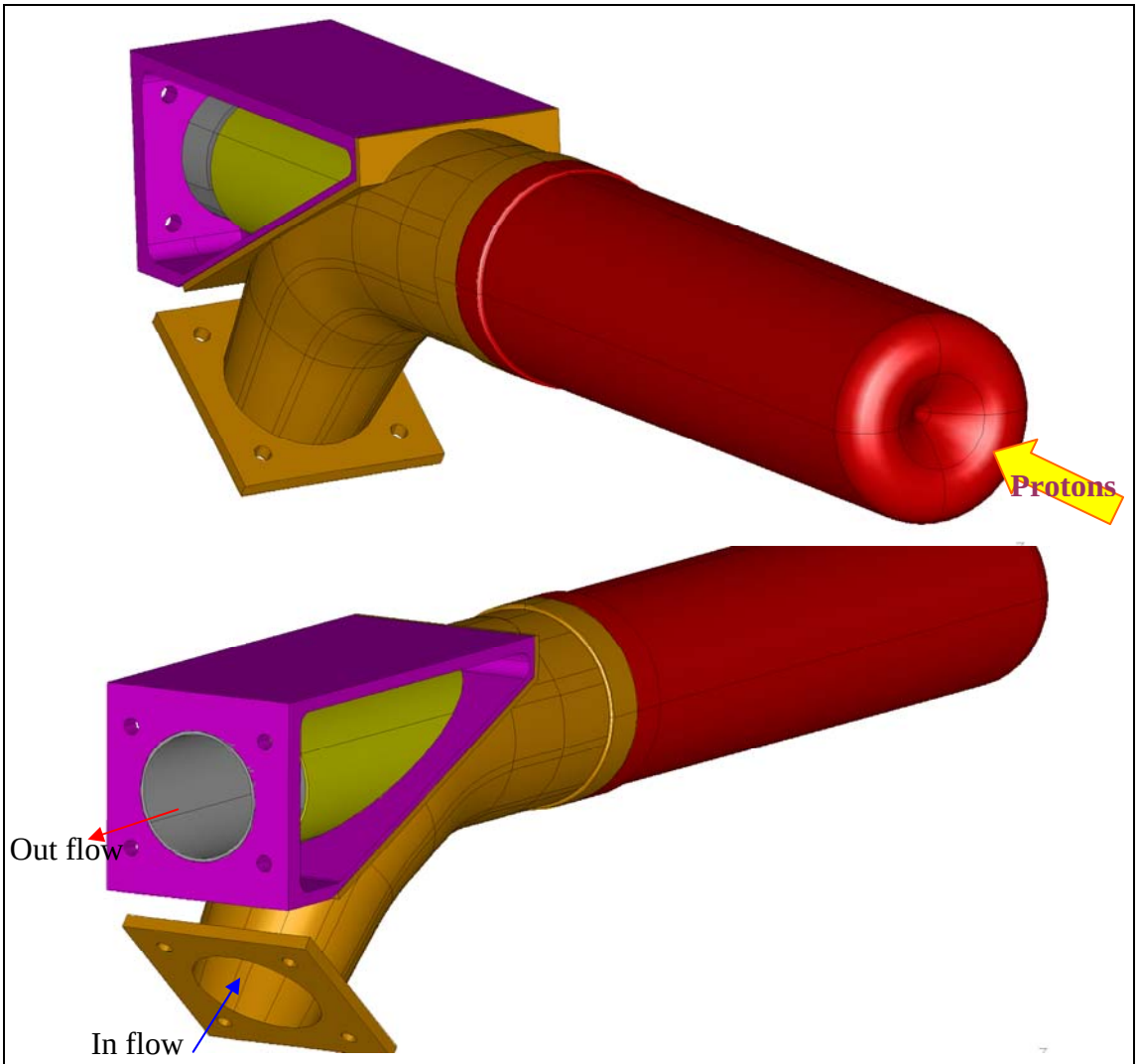

Figure 4-2. Eurisol Converter target optimised design

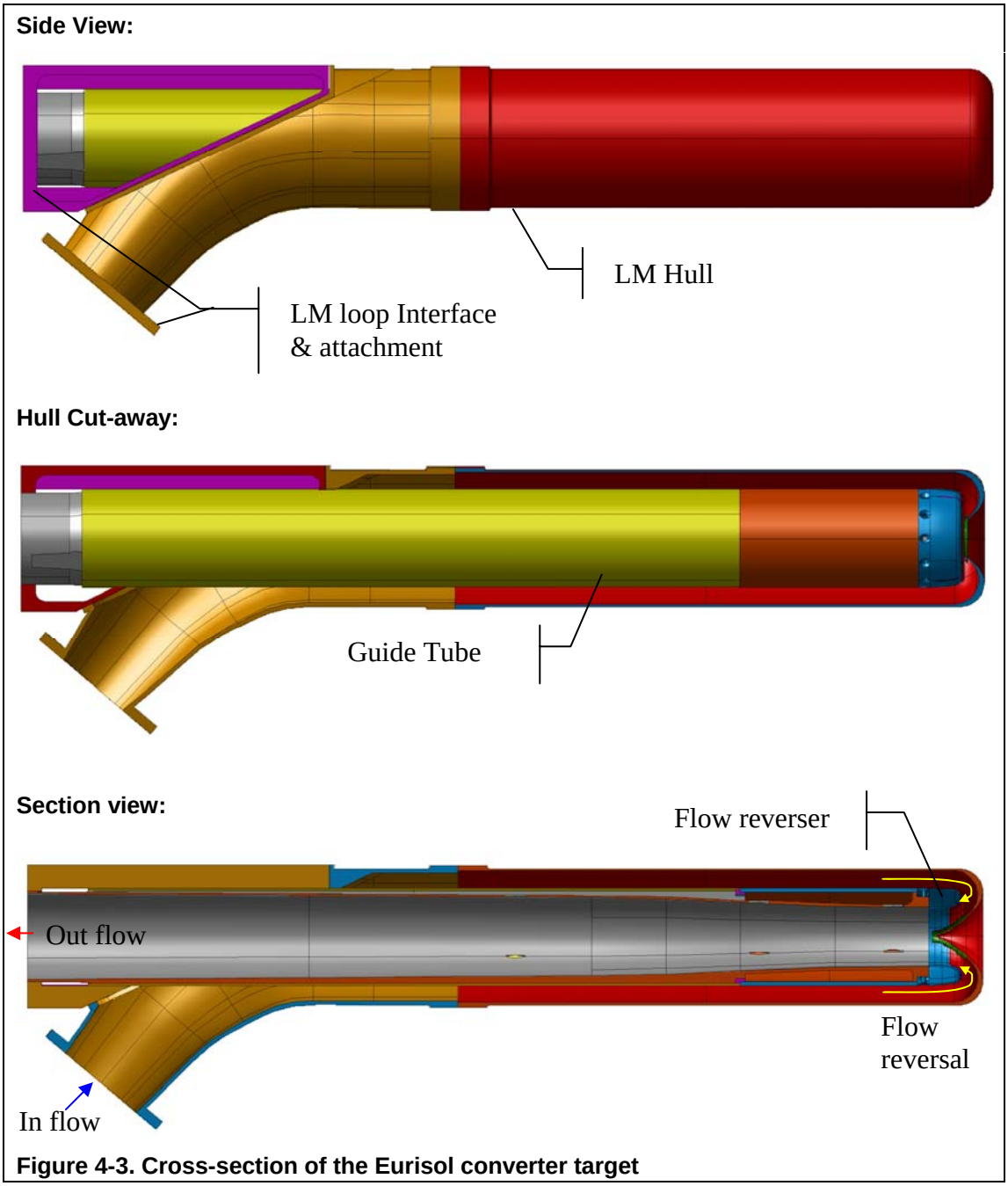

Figure 4-3. Cross-section of the Eurisol converter target

The design contains a number of improvements which cover most if not all of the goals set out above. The next following pages will explain how the converter target can be manufactured, and the operational aspects of the converter target. Calculations in chapters 5 and 5.2 serve to quantify numerically the expected benefits and operational modes of the target.

4.2.1 Attachment interface to LM loop

The rear of the target is attached to the shielding block where all the connections to the LM loop are placed. The LM reaches the rear of the target through pipes imbedded in the 4m thick shielding block, represented partially in Figure 4-4 for clarity (In reality it extends 4 m to the left of the back end of the target, and in the vertical plane as well).

The inflowing LM enters the target from below at a 30 degree angle. This solution seems to offer the best compromise in terms of simplifying interfaces whilst minimising pressure losses. Another option would have been to design a co-axial annular interface surrounding the outlet as such a solution would have resulted in less friction loss but it would have complicated the task of attaching/detaching the target.

The LM flowing out of target exits through a circular co-axial outlet which interfaces with a similar diameter pipe on the LM loop.

Thus; in the proposed design, there are two separate 100mm diameter circular pipe sections meeting with the LM loop. The basic philosophy for interfacing with the LM loop is to define the target position in the vertical plane by inserting the back end into the rails as shown in Figure 4-4. It is then slid it into place to match up with the angled interface in such a way as to ensure a perfect fit on both interfaces.

The design is such that the vertical and angled interfaces are not rigidly connected to one another on the target side. This should give enough compliance for the inevitable tolerance mismatches to be compensated for without excessive clamp-down stresses.

It should be emphasized however that the LM loop structure the target attaches to must be perfectly rigid on both the angled inlet and vertical outlet interface. If that is not the case, there are bound to be serious problems with resonance frequencies excited by the high LM flow.

Both the inlet and outlet interface need to be properly sealed, a subject which has not yet been fully studied. Indeed the hardware being produced for the hydraulic test will feature conventional polymeric gaskets. In a production target the seals would have to be integrated to the interface to facilitate operations. An inflatable metal seal or a captured Cefilac® spiral-wire seal may be a solution, but have not been looked at in any detail at this stage in the design.

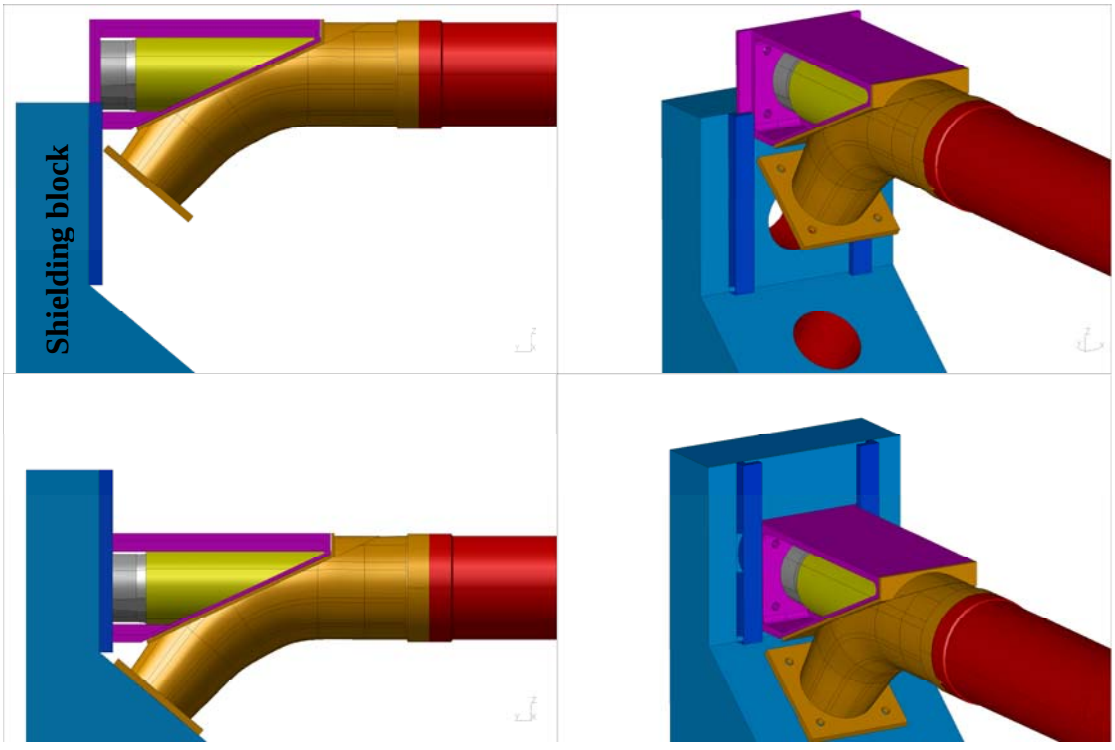

Figure 4-4. Steps in integrating the converter target to the LM Loop

Shielding block not shown in full length or height to visualise integration more easily

4.2.2 Inlet / Outlet channel and thermal barrier

Insulating the cold inflowing LM from the heated outflow is necessary to facilitate heat extraction from the converter target but it is also complicated due to space limitation imposed on the design. In addition pressure must be minimised because of the restrictions on the pump.

The solution to this particular problem relies on LM flowing into the target from below at 40° to the horizontal to improve hydraulic efficiency. The inflow is thermally insulated from the LM flowing out by a double-walled guide tube structure, the cavity between the two walls being filled with air.

The double–walled guide tube is essentially manufactured from an inner machined barrel with ribs on the outer surface over which a simple outer tube is positioned and welded in position (see detail in Figure 4-6). Thus the only full thru-metal thermal passage from the outflow to the inflow side occurs along the ribs, which represent less that 10% of the total wetted surface. Although this design does not eliminate thermal cross-flow entirely it does limit the extent of the problem.

The inflow channel is defined by the outer shell (in yellow in Figure 4-5) of the guide tube which is welded to the support piece (magenta) as shown in the figure below. Then the inlet tube (orange) is welded on the support piece. Thus the inflow channel is formed whereby the LM entering through a circular pipe section flows either side of the guide tube and then co-axially towards the window.

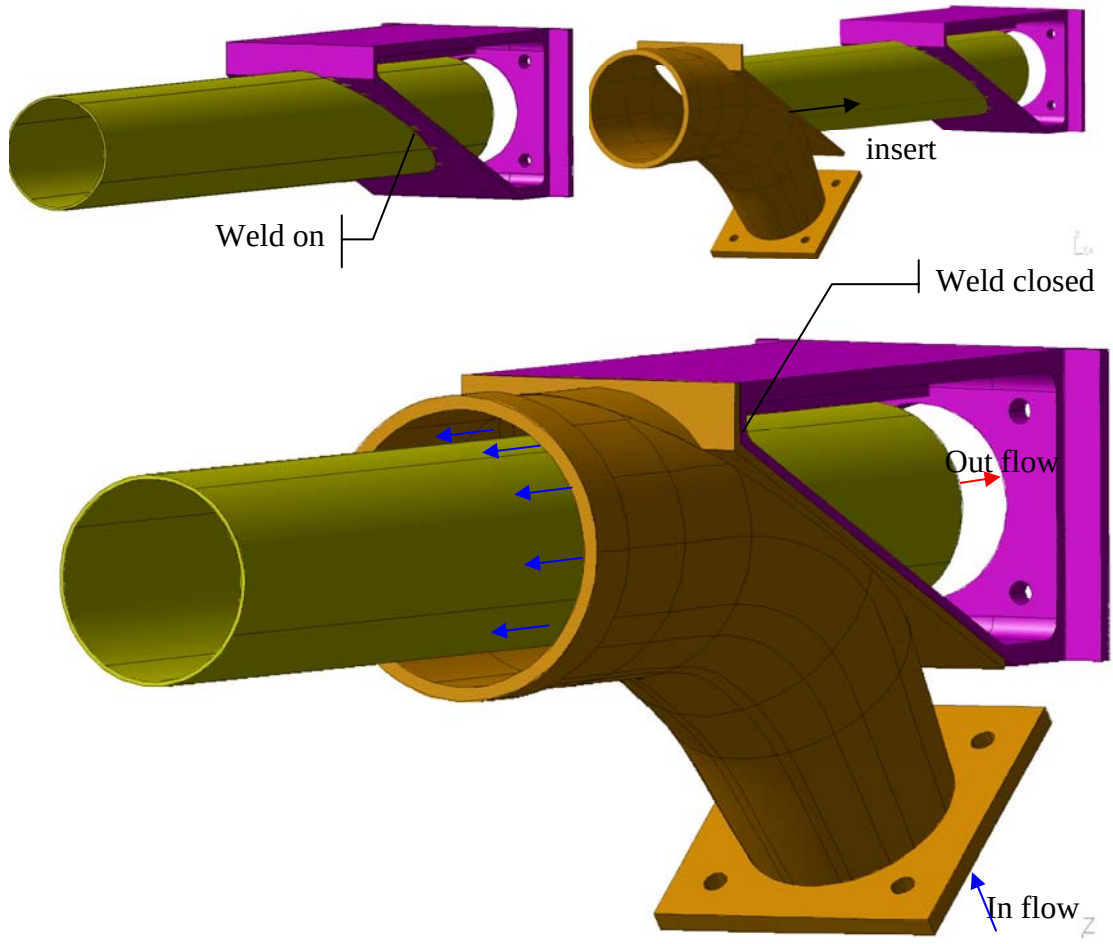

Figure 4-5. Manufacturing of the inlet channel

The return flow of LM towards the back of the converter target is directed by the inner guide tube (in gray in Figure 4-6 below). The guide tube is essentially hollow, formed by an outer cylindrical tube (yellow in Figure 4-6) which is welded onto the machined inner guide tube. The ribs of the inner guide tube maintain a small thermal gap between the outer cylinder and the inner guide tube (detail in Figure 4-6). In addition the inner guide tube features three channels spaced out at 120° which serve to house the instrumentation cabling leading back to the rear of the target where transducers for the pressure pick-ups and electronic data gathering are located. The fore part of the guide tube has a large cavity to prevent heating from the proton beam.

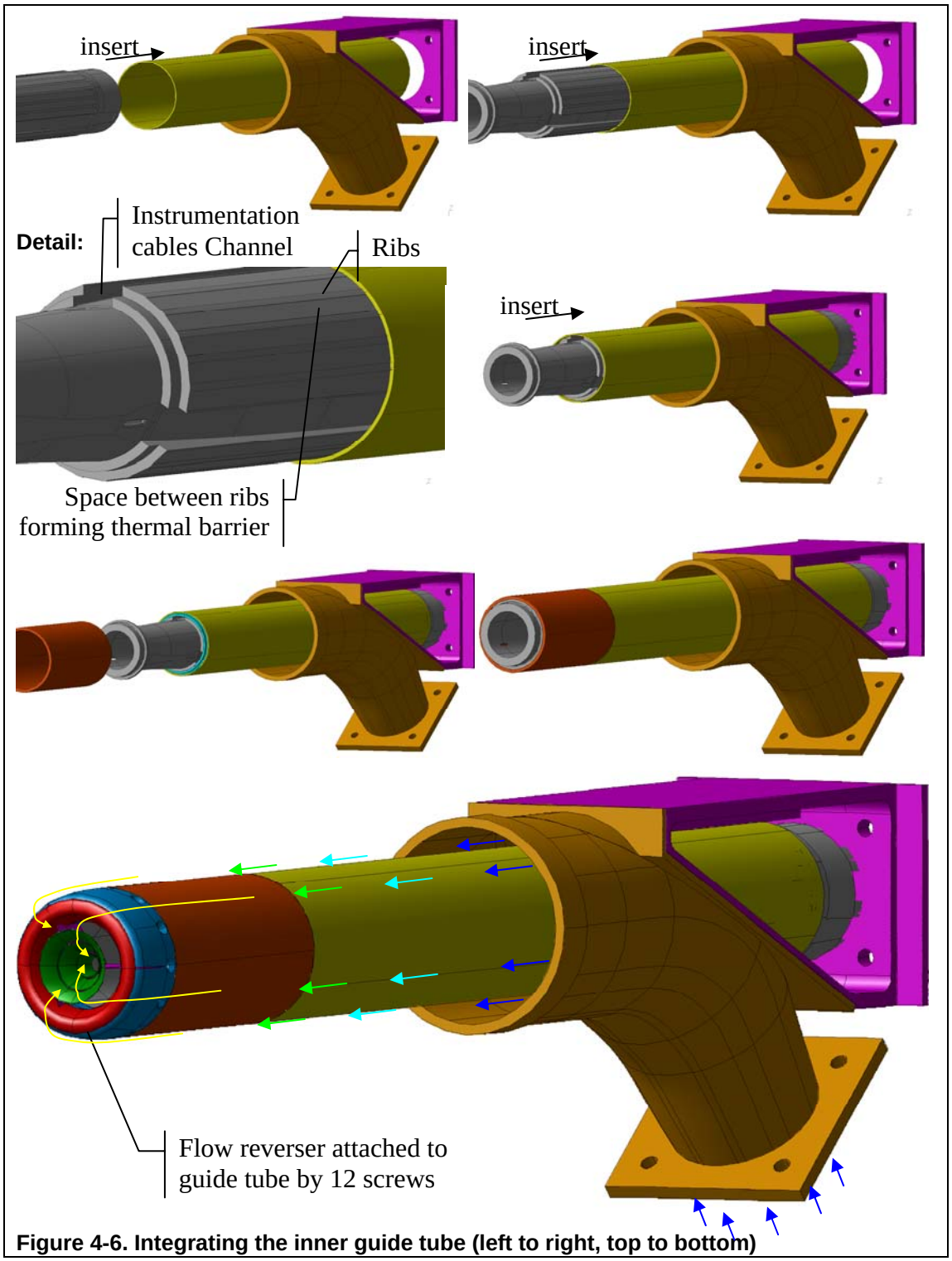

Figure 4-6. Integrating the inner guide tube (left to right, top to bottom)

4.2.3 Flow reverser

The purpose of the flow reverser is to turn the flow 180° with minimal pressure loss. At the same time it should encourage convective cooling by accelerating and attaching the flow locally over the window.

Figure 4-7 below shows how the reverser is manufactured. First, the 3 supports for the flow vanes are welded into three matching slits spaced out at 120° in the fore end of the guide tube which is detachable. The latter piece resembling a cowling attaches to the guide tube by a dozen screws at 30° pitch, which enables the flow reverser assembly to be rotated by 30° relative to the static instrumentation inside the guide tube. Thus by simply rotating the flow reverser, different velocity profiles of interest can be measured either between or directly behind the 3 supports.

Once the supports are in place the vanes immediately adjacent to the widow surface (shown in green below) can be welded on. The window vanes are intended to accelerate the LM locally over the hottest part of the window where the proton beam enters the target; there are three vanes separated by small slits between them. This helps reduce pressure losses by allowing some of the LM which is being compressed against the window to escape into the return flow inside the guide tube, where it can accelerate the main flow in an area of high heat deposition.

Initially the window vanes form a single funnel shaped piece (not shown here). The slits between each individual vane are only machined in after the vane funnel has been welded on. The basic idea is to prevent distortions during welding, as the whole funnel-shaped piece ought to be stiffer than 3 separate vanes.

Finally the vane on the guide tube cowling (in red below) is welded on. It is thicker in section than the window vanes and has a dual purpose; on the one hand to help bend the flow back into the guide tube, but also to reduce cavitation risk on the back-swept part of the guide tube by encouraging reattachment of the flow.

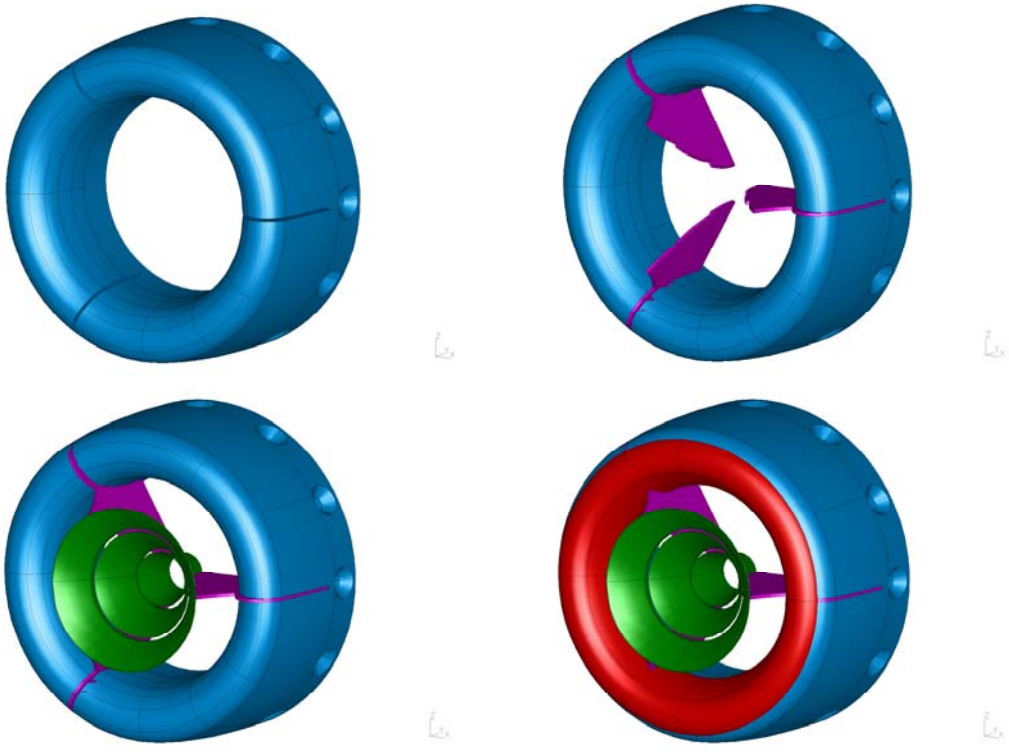

Figure 4-7. Steps in manufacturing the integrated flow reverser unit (left to right, top to bottom)

4.2.4 Instrumentation

Instrumentation is only relevant to the target manufactured for the hydraulic test. It is not intended for the production unit which will at most contain a few thermo-couples, but no pressure pick-ups for velocity profiling.

The method for measuring the velocity profiles relies on conventional Pitot tubes housed in winglets which are inserted at three stations along the return flow in the guide tubes as shown in Figure 4-8 below with the tubes running towards the rear of the target in dedicated instrumentations tunnels, this instrumentation harness is repeated three times around the circumference, spaced out at 120° intervals.

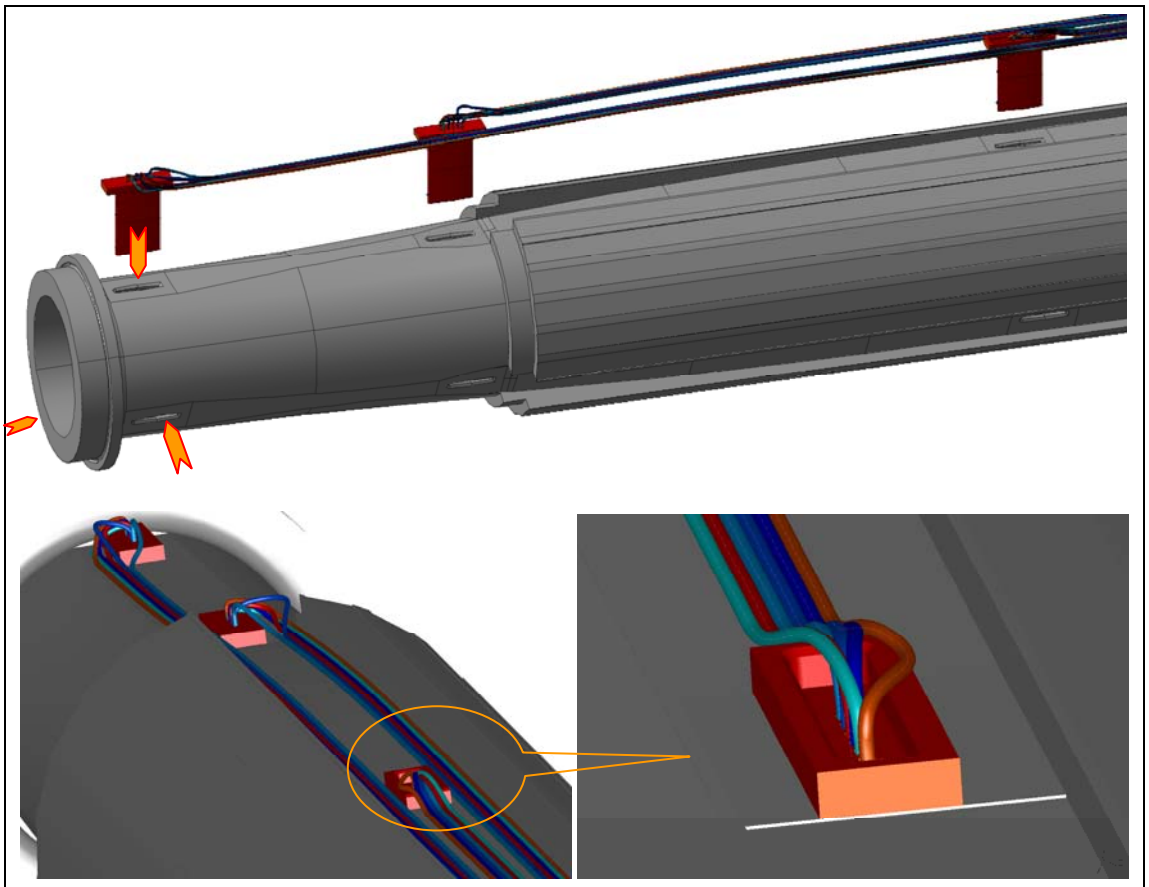

Figure 4-8. Positioning of the instrumentation in the guide tube

The winglets contain not only capillary tubes for pressure pick-up but also thermocouples so as to resolve the thermal boundary layer as well as the velocity boundary layer.

The thermocouples and capillary tubes are both 1 mm in diameter and sufficiently pliable to be bent around tight radii. Nevertheless, care must be taken when routing the tubes particularly at the rear station where the thickness of the guide tube is very much reduced and does not offer much space. As shown in the bottom right of Figure 4-8, it may be necessary to hollow out the pad on the rear most winglet to give sufficient space for bending the tubes.

The winglets have all been placed in line for the time being. Further CFD analysis is needed to check whether the second station is not adversely affected by the downwash from the first station. If that is the case there are two possible solutions; the easiest from a design point of view is to offset laterally the centreline of the second winglet by about 10 mm from that of the first. If this is not enough, the second

possibility is to create a set of instrumentation tunnels every 60° so as to place the second row of winglets 60° offset from the first respectively last row.

The following figure gives some insight into the manufacturing and internal details of the winglets containing the pressure pick-ups and thermo-couples. All pressure measurements are made at the rear of the target via the capillaries which run out to pressure transducers. On each winglet there is a pressure pick-up in the dead zone at the base of the trailing edge to measure static pressure. There are three pressure pick-ups on the leading edge so as to resolve the velocity boundary layer.

In addition two thermocouples; one near the wall and one closer to the centreline allow measurement of the thermal boundary layer, when tests with heated LM are carried out, although this will not take place in the first test campaign in early 2008.

The manufacturing of the instrumentation winglets is illustrated in Figure 4-9, starting with the placement of the thermo-couples and capillaries in grooves that have been previously machined in a flat plate. A second plate is placed on top and the whole assembly is brazed creating a solid block using high-temperature soldering techniques. Care must be taken during soldering not to obstruct the capillaries with flux; this may be prevented by allowing a small extension length of capillary out of the block which ensures they remain open after they have been machined back.

Finally the soldered block with the imbedded capillaries and thermo-couples can be machined in the shape of a winglet with an attachment pad, all the tubes protruding from the lower end of the pad.

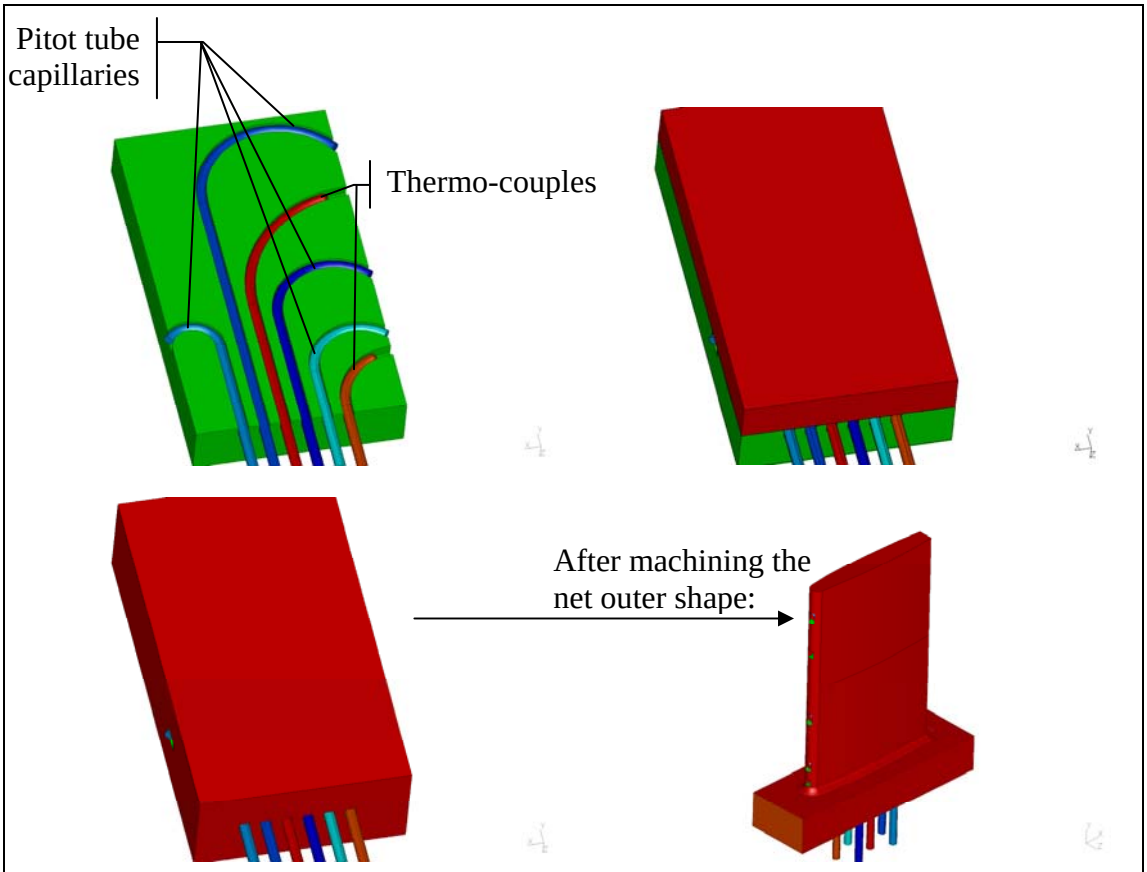

Figure 4-9. Steps in manufacturing instrumentation winglets (left to right, top to bottom)

4.2.5 Outer hull

The outer hull is simply welded on to the inlet tube at a thickened section. Although the final strategy for the window has not yet been decided it may be feasible to foresee a bolted flange in lieu of the weld as this may facilitate the exchange of damaged outer hulls, particularly in the window area.

Overall, the nature of the connection from the outer hull to the inlet tube does not affect the hydraulic performance inside the target, hence the present design study does not consider it in any greater detail, but leaves the choice open to the draughtsman as to the exact nature of this interface, bolted, welded or indeed even secured with a belt-clamp.

The exact dimensions of the window hull shape have been derived with a full thermal-hydraulic analysis for a σ 15mm beam, some preliminary work exists for a σ 25mm beam indicating the minimum thickness could be increased from it's current value of 0.8 mm at the tip of the cusp to about 1.7 mm. The main differences are summarised in the figure below for completeness.

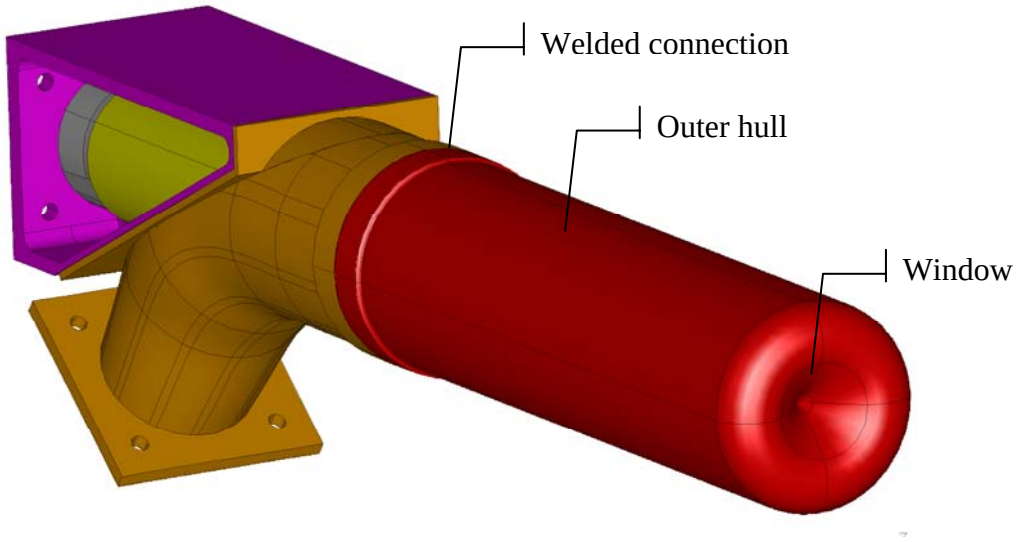

Dimensions defining the cross section of the cusp-shaped window for a σ 15mm beam

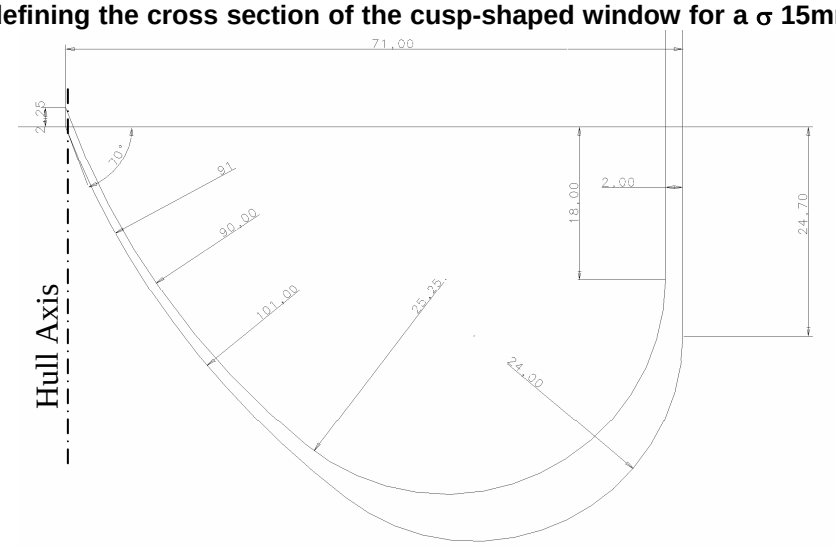

Figure 4-10. Design of the outer hull

5 Structural analysis of the converter target

The structural integrity of the target is influenced by many operational aspects, first and foremost the proton beam which deposits a power of 4 MW in a volume the size of a teapot. This leads to severe thermal stresses at the point of entry. In addition the protons tend to modify the characteristics of the material with increased irradiation time.

There are other distinguishing features in the converter target such as dealing with the hydraulic impact of circulating large amounts of heavy liquid metal; Hg has a specific gravity of 13. The main concerns in this particular instance are exciting resonances in the structure, erosion / cavitation of the wetted surfaces, and the habitual stress issues linked to the necessity of pressurising the loop to prevent boiling.

These different areas of concern are briefly addressed in the following section. A concatenation of existing analyses and new results is presented to provide the reader with as complete as possible an overview of the analysis required to validate the concept described in the previous chapter.

5.1 Stress analysis of the window area

5.1.1 Thermal stresses caused by a beam centred on the window

The stress analysis of the window has been conducted in 2D with a section model which uses axis-symmetric elements, i.e. elements which react a normal radial pressure load in the 2D plane of the element by circumferential (hoop) loads out-of-plane of the element. Such elements are only suitable if the boundary conditions, and in this instance the proton beam heat deposition, is axis-symmetric. Otherwise in cases where the beam is off-centre, a full 3D analysis is necessary.

The main contribution to the peak von Mises stress in the window shown in Figure 5-1 is bending caused by differential thermal elongation on the LBE wetted surface compared to the outer surface which is not cooled. The magnitude of the stress is 25 % lower than the allowable value at the corresponding operational temperature, for an irradiation limit of 2 [dpa] (refer to section 3.5.1, page 12)

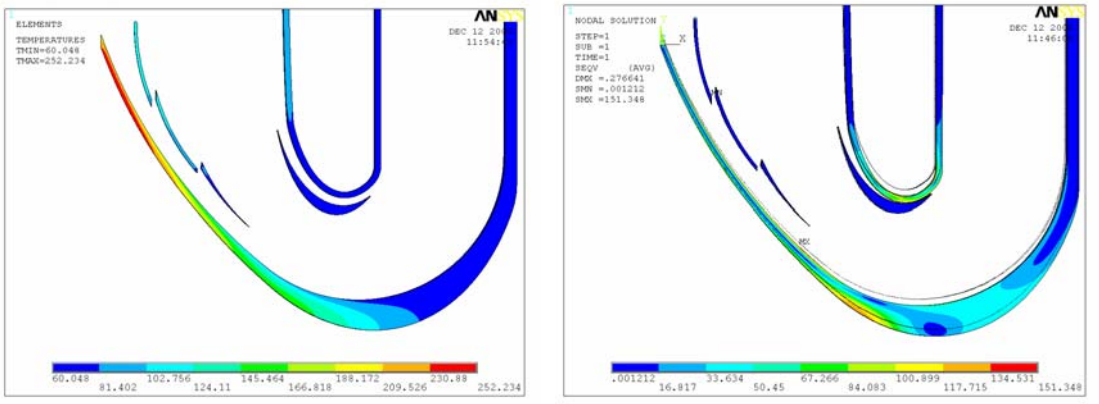

Figure 5-1. Thermal stresses on the window of the outer hull from [Ref3]

(Shadow line indicates original vs. displaced shape in right figure)

5.1.2 Pressure stresses combined with thermal stresses

As in the section above, the analysis of the 10 [Bar] pressure case has also been conducted in 2D with axis-symmetric elements. Note that the 10 [Bar] value contains a safety factor of 2 on the nominal systems pressure in the loop, which is 5 [Bar] (§3.2 page 10). The pressure has been applied as a surface load along the inner surface of the hull.

Most notably, the peak Von Mises stress diminished by 15 [MPa] for an applied pressure of 10 [Bar], the reason being that the peak thermal stress is a tensile stress in radial direction on the inner surface. Thus, when pressure is applied to the cusp, the resulting reaction compressive stress over the section adds to the existing stress state from the thermal elongation, such that the tensile thermal stress is reduced on the inner surface. Conversely the compressive stress existing on the outer surface is increased, such that the peak von Mises stress (which is the magnitude of the stress tensor) appears on the outer and no longer on the inner surface. The compressive thermal stress on the outer surface being lower in magnitude than its tensile counterpart, the net effect is a decrease in the overall level of Von Mises stress in the window.

Pressure load (red arrows) **Von Mises stress on displaced shape (5x)**

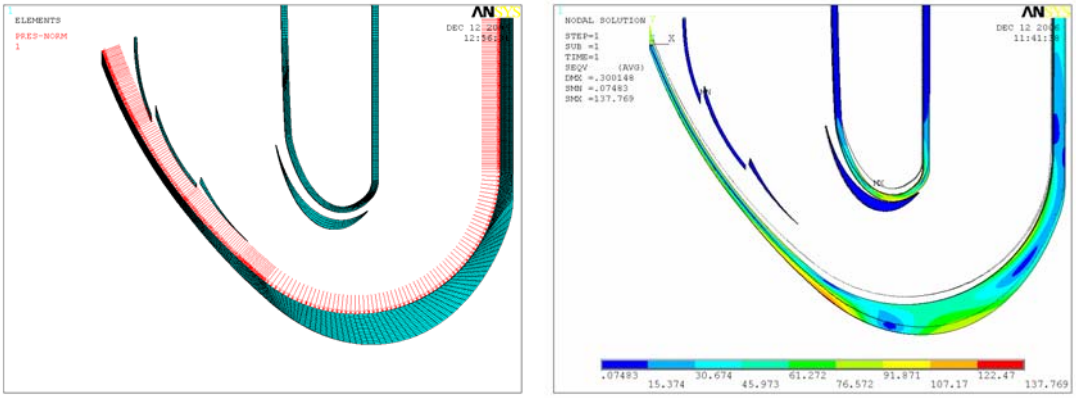

Figure 5-2. Thermal + 10 Bar pressure stresses on the window of the outer hull from [Ref3]

(Shadow line indicates original vs. displaced shape in right figure)

5.1.3 Thermal stresses caused by a beam off-centre by 5 mm

The thermal stresses caused by an off-centre beam cannot be calculated with an axis-symmetric model. Indeed if the heat deposition were offset in such a model, the load that would be considered in the model would be a torus and not a circular spot.

In order to calculate the stresses in such a case a 3D model has to be set up. Half symmetry may be used to diminish the size of the model, as long as the centre of the beam is shifted along the symmetry plane. Although results exist for the CFD and hence the temperature distribution, no analysis of the stresses has been conducted at this stage.

5.2 Resonance analysis of critical areas in the target

The density of the LM inside the converter target is very high (specific gravity 13). The structure must therefore be sufficiently rigid to prevent natural resonance of the structure to be excited by the LM circulating at high speed.

A rough goal which can be set to preclude the possibility of resonance coupling between the fluid and the structure is to ensure that any significant Eigen frequency of the structure remains above 100 [Hz]. Although not set in marble, this limit is useful in the design stage of a structure as it ensures that the Eigen frequencies remain in a range where they are only likely to be the cause of “buzzing” rather than any significant oscillation which could lead to structural failure.

The next following paragraphs will examine some of the structure deemed to be most at risk in the event of resonance coupling.

5.2.1 Eigen-frequency of the flow reverser

The flow reverser has been singled out as particularly susceptible to resonance as it is located precisely where the flow is reversed and hence turbulence can be expected. Furthermore the structure of the flow reverser is undoubtedly one of the more flimsy in appearance, compared to the rest of the target structure.

An Eigen-value analysis is conducted on the flow reverser wherein it is clamped rigidly at the base of the three supports. This assumption is very pessimistic, as in actual fact the supports slot into grooves of the flow reverser cowling piece and are maintained rigidly laterally. Despite this pessimistic assumption the frequency remains high at 896 [Hz]. The next frequency stands at 1297 [Hz].

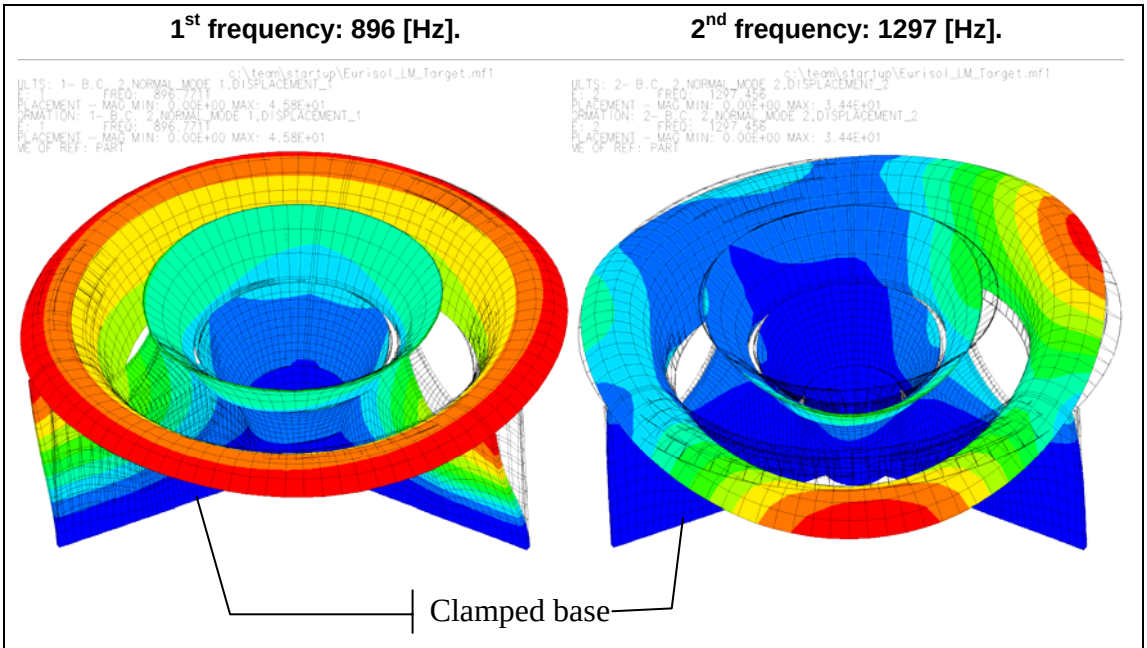

Figure 5-3. Normalised resonance shapes of the flow reverser clamped at the base of the three supports

The effect of the heavy LM surrounding the structure is not taken into account in the previous calculation. In reality the fluid surrounding the structure will resonate with the structure and add its mass, thus decreasing the natural frequency of the whole. Inevitably this effect is a coupled fluid-structure problem, which may not be solved by Eigen-value analysis. The magnitude of the shift in frequency can be

estimated however by simply adding on the mass of the fluid surrounding the structure. This assumption is pessimistic, as in reality the fluid also has a viscous effect which helps alleviate some of the stress concerns caused by structural resonance.

A second Eigen value analysis is therefore carried out, where the total mass of the fluid in the window area surrounding the flow reverser is added to the structure as a distributed mass. The support is this time clamped along its side, which is more realistic given the supports slot into the guide tube. The volume of fluid considered in the analysis, which weighs 10.26 [kg] is shown on a segment in Figure 5-4 below.

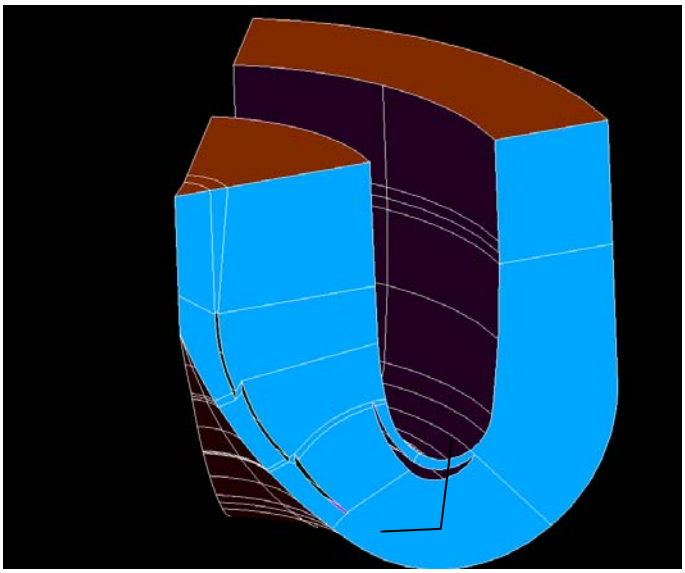

Figure 5-4. Mass of fluid surrounding the flow reverser assembly used in the modified Eigen-value analysis

The shift in frequency is then quite apparent as shown in Figure 5-5 below. The first Eigen-frequency drops to 225 [Hz]; high enough to be considered too rigid for any resonance to be activated by the fluid.

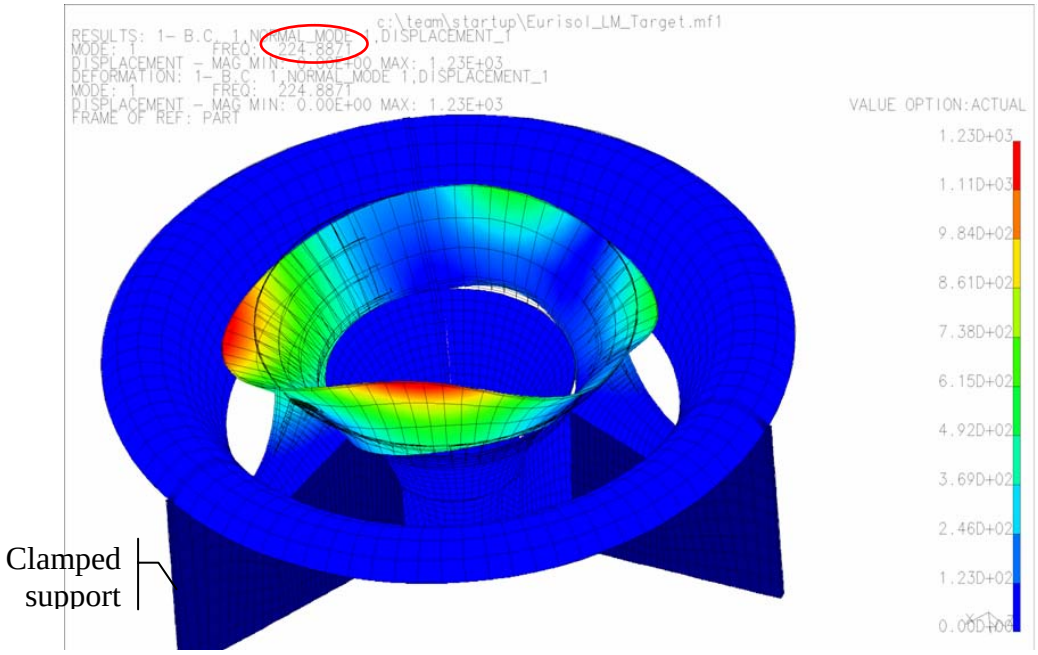

Figure 5-5. Normalised resonance shape of the flow reverser with added fluid mass

5.2.2 Eigen-frequency of the outer hull

The outer hull supporting all the mass of the LM is another item of concern. Particularly as the converter target is only supported at the rear end. The mass of the LM inside the target is therefore added as a distributed mass onto the outer structure of the converter target, the inner structure such as the guide tube is not assumed to add any rigidity to the assembly.

The mass of Mercury contained in the fore part of the hull, extending from the cusp to the foremost station of the attachment structure amounts to approximately 90[kg]. This mass can conservatively be assumed to oscillate with the structure of the hull and is therefore added as a uniformly distributed mass of roughly 300 [kg/m^2] on the FEM model plate elements which form the outer shell of the target structure.

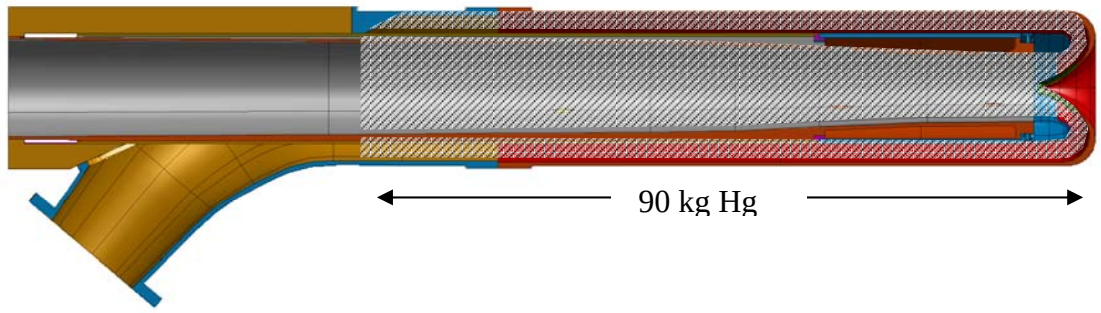

Figure 5-6. Resonance of outer hull added LM mass

A shell model of the outer structure, complete with the attachment interface is set up to calculate the Eigen frequencies of the structure. The first three frequencies are depicted in Figure 5-7 below and show resonance starting at 42 Hz.

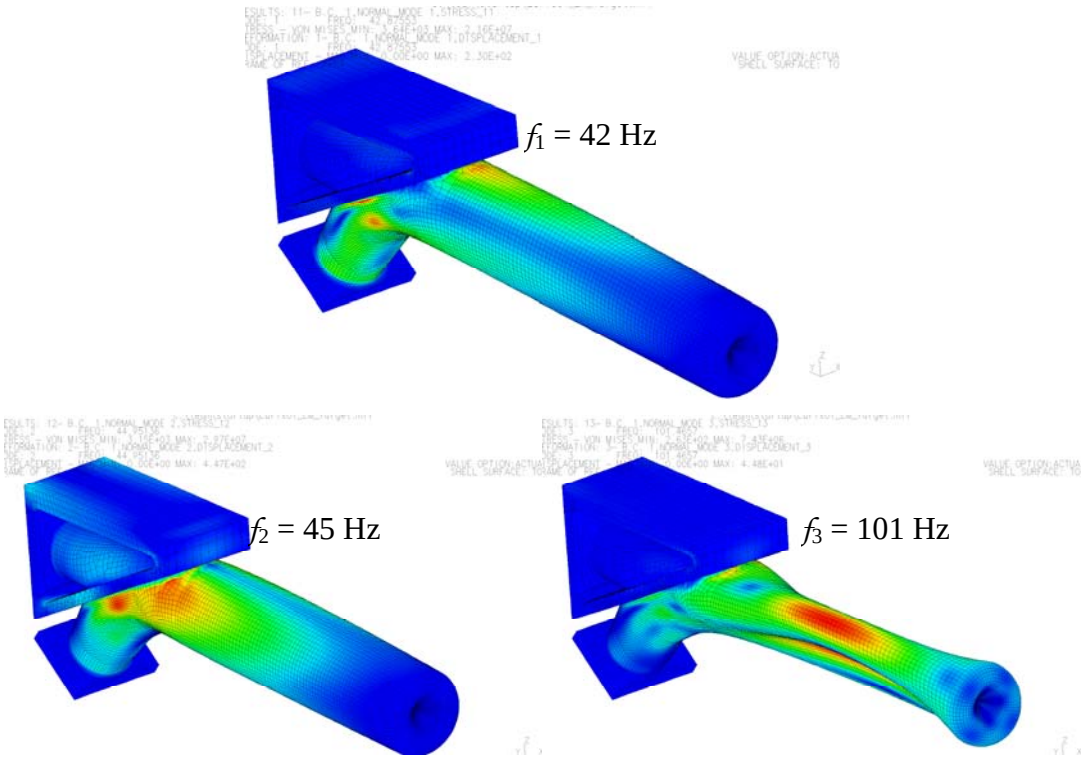

Figure 5-7. First three natural frequencies of the outer structure with added LM mass

Note: contours show mass-normalised stress, hence indicative of relative value only

The first mode is a bending mode in the vertical plane. This results in stress concentrations where the outer hull meets the supporting bracket. The next mode is a lateral bending mode, and finally the third mode is an ovalisation of the circular hull section.

The first two modes are clearly below 100 [Hz] and need to be examined closely. The inflowing LM will have a component which could well activate the first vertical mode. The second mode is lateral and is therefore unlikely to be excited as there is no large velocity component of the LM in that direction. It is therefore prudent to seek to stiffen the structure as far as possible against the appearance of the first vertical bending mode.

It is also important to minimise the stress concentrations occurring in the hull and which show up in Figure 5-7. The magnitude of these stresses is unknown, as the Eigen value analysis is mass-normalised and the stress values in Figure 5-7 are only indicative in relative terms not absolute. For absolute stress values to be determined it would be necessary to conduct a coupled dynamic analysis whereby the power contained in the turbulence of the LM flow is extracted and applied as a Power Density Spectrum (PSD function) to a dynamic structural model of the hull.

A simplification of the problem is proposed here, limited to evaluating various means of stiffening the structure so as to increase significantly the vertical bending mode. This is achieved as shown in Figure 5-8 by increasing the hull thickness from 2 to 2.6 [mm] and adding stiffeners. The first frequency appears at 62 [Hz], however it is lateral mode. The vertical mode, the one which is of major concern is increased from 42 to 83 [Hz]. Given the conservatism in the approach, such an improvement in vertical stiffness is sufficient.

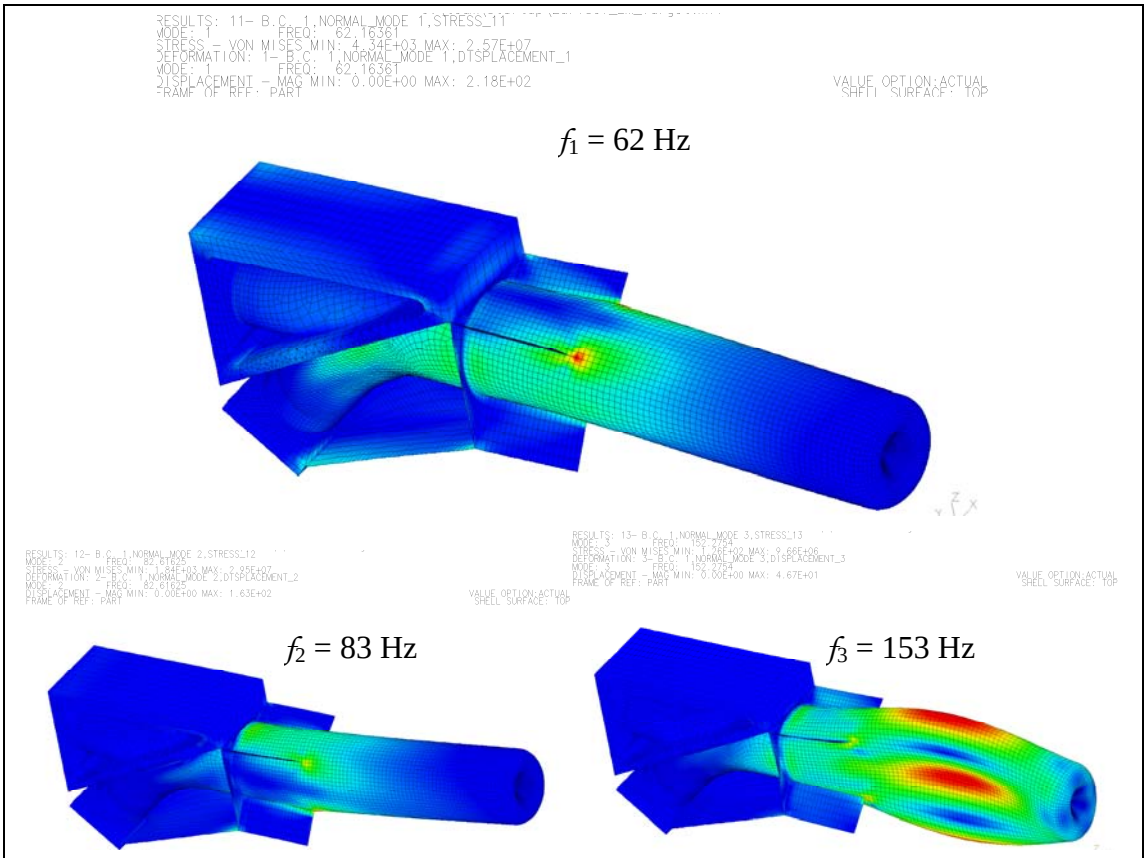

Figure 5-8. First three natural frequencies of the outer structure with stiffeners

Note: contours show mass-normalised stress, hence indicative of relative value only

The improvements required to increase the stiffness of the outer hull structure are shown in Figure 5-9 below, in schematic form based on the FEM results. It is desirable that as much as possible of the added stiffening be included in the final production version of the converter target. However this is subject to geometric and interface constraints, so that it may be necessary to give up some of the suggested improvements for interface reasons.

There is no stiffening of the outer hull structure in the design description or the CFD analysis contained in this document, since the extent of the stiffening to be implemented is subject to further discussion pending review of interface issues, This matter does not affect the hydraulic or thermal performance of the converter target and can be decided on independently at a later stage.

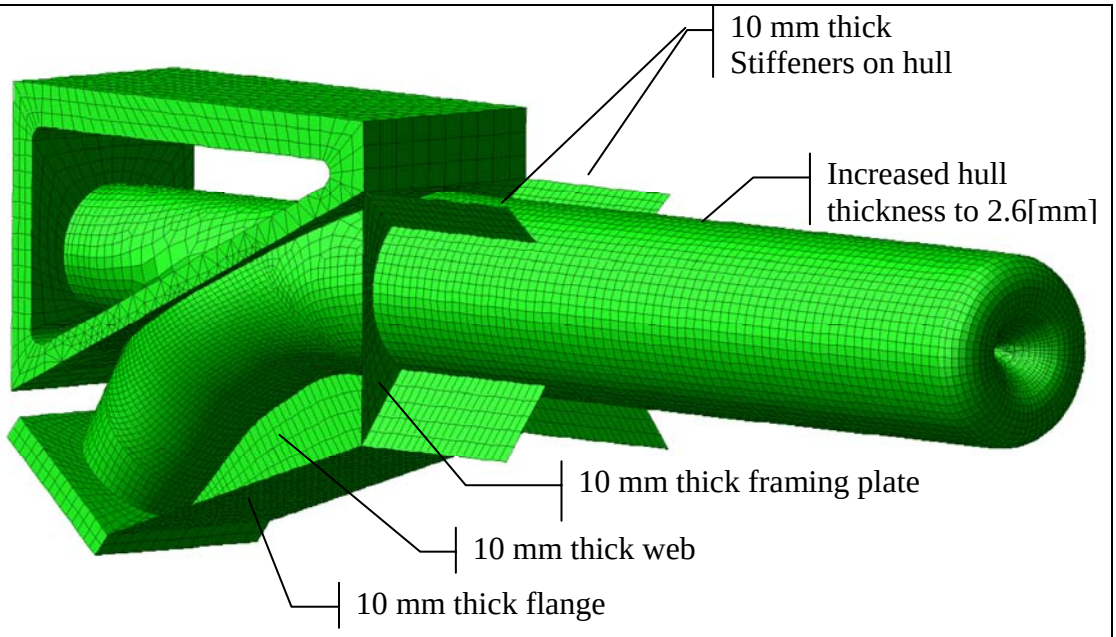

Figure 5-9. Stiffened structure improvements

CAUTION

In light of the results above it should be stressed that in the upcoming hydraulic test;

BOTH INLET AND OUTLET INTERFACES MUST AT ALL TIMES BE SECURELY CLAMPED DOWN.

It would be unadvisable for instance to fasten only the outlet and leave the inlet floating.

6 Fluid dynamic analysis of the converter target.

The CFD analysis conducted in past successive iteration to arrive at a final design were all based on 2D sectional models. These models were sufficient to conduct trade-off studies, particularly in the window area which is the most critical to the design.

It is however necessary, for a full and complete analysis of the optimised design, to examine cases which are not axis-symmetric. The inlet for instance, is not geometrically symmetric. Yet the hydraulic phenomena and thermal exchange of the inlet flow with the exiting co-axial outlet flow are areas significant matters for an accurate prediction of the performance of the converter target. The effect of the beam wandering off-centre also bears considerable importance from an operational perspective to ensure that in such circumstances the cusp-shaped window is not adversely affected in terms of temperature or stress.

6.1 Detail 180 degree segment model of the window area.

A 180° segment model of the window is set up to study the effects of gravity and buoyancy, the consequences of an off-centre beam, and the flow around the vane supports.

6.1.1 Model Description

The model is focused on the window area only as shown below in Figure 6-1 and is nevertheless quite large.

Number of elements:	1 372 927
Wedges (Pentahedrons):	15 265
Bricks (Hexahedrons):	1 357 662

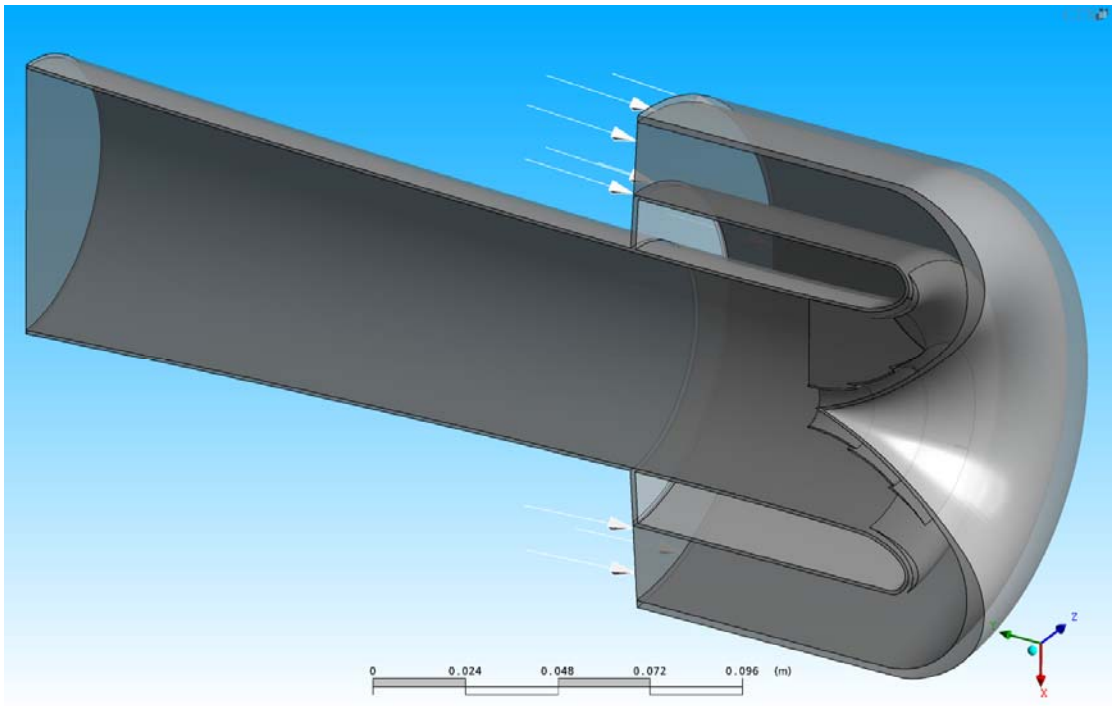

Figure 6-1. 3D model of the window area

The inlet channel has been cut off as it is not of primary importance and the model concentrated on the most vital parts of the window, including half-symmetry to reduce size. Nevertheless, the model is inevitably much larger in 3D than in the section models. It is necessary to also optimise the number of elements in a section quite carefully so as to minimise computational expense. Based on prior experience the areas needing most definition are well known and concentrated on the hull window the vanes supports and the vanes, as shown below in Figure 6-2.

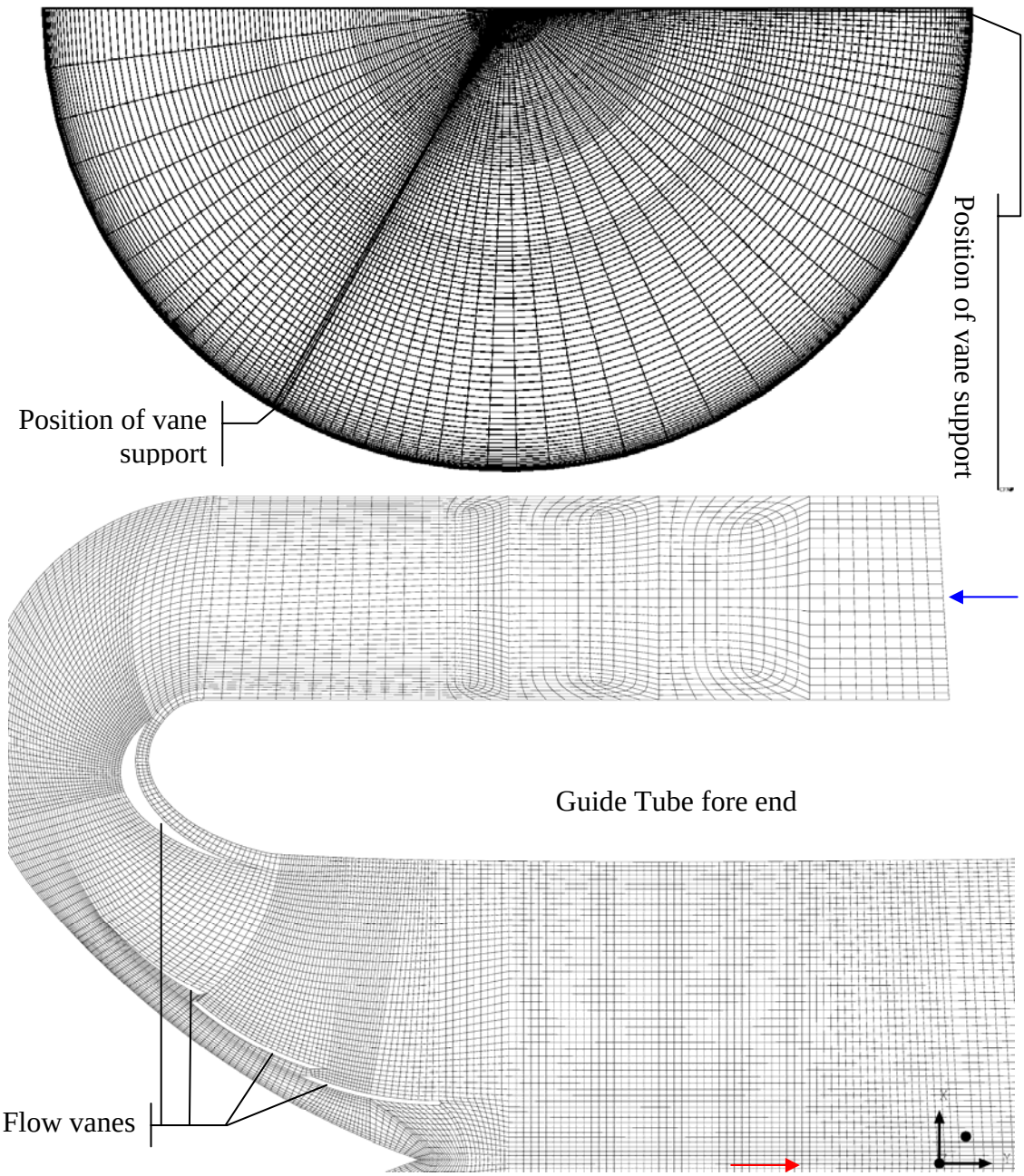

Figure 6-2. Close-up of the element definition in section (top) and in the window (bottom)

The turbulence model is the SST used previously quite successfully. Medium instability (5%) was selected for the inlet turbulence. A transient analysis is run with the proton beam switched on immediately at time 0, the time step selected is 0.1 [ms] and the model is run for 1 [s] sufficient to reach saturation and detect any instability in the flow.

6.1.2 Beam centred on the window

The analysis of the nominal case with the beam centred on the window is important to assess the stability of the flow, the three-dimensional cooling the window and the effect of buoyancy.

The temperature distribution in the LM and structure follows the pattern observed in the two-dimensional analysis reported on in section 5.1.1. In particular there is good agreement between the two models on the temperature distribution in the window (Compare Figure 5-1 and Figure 6-3 below).

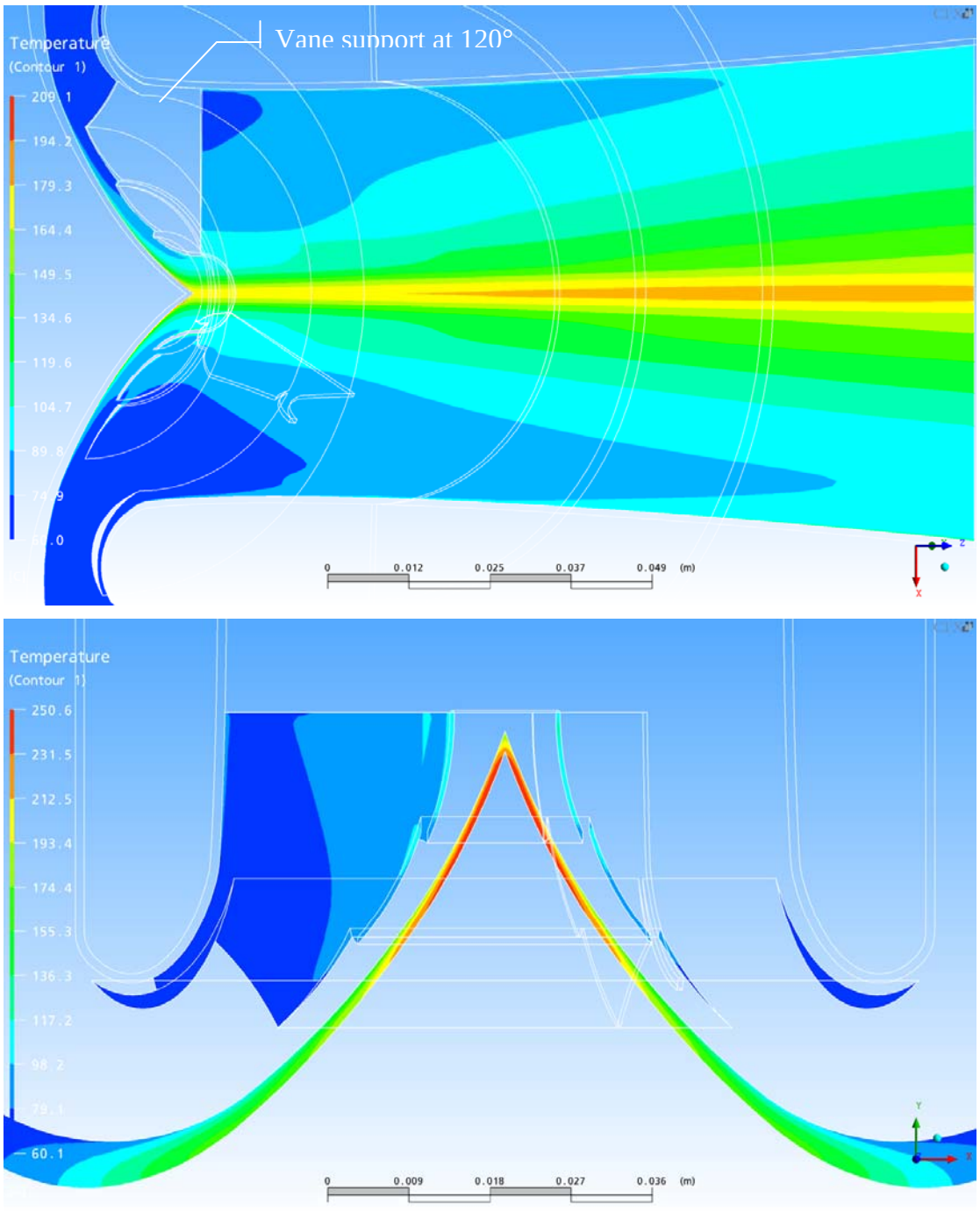

Figure 6-3. Detail of the temperatures in the LM (top) and structure (bottom)

One of the vane supports intersects the symmetry plane, such that the structure of this support shows up in the section view in the lower portion of Figure 6-3. The

centre of this support does not exceed a temperature of 120 C nor does any of the vanes. The flow deflector structure is therefore well cooled and should not distort under thermal expansion. It may however shift slightly in terms of position relative to the window as the window expands. However since the bulk of the structure is well cooled this distortion will remain limited.

One of the purposes of the three-dimensional CFD analysis is to show how the flow is distributed around the vane supports. Figure 6-4 below shows the streamlines leaving the inlet at positions that are in line with the two vane supports at 0° and 120°.

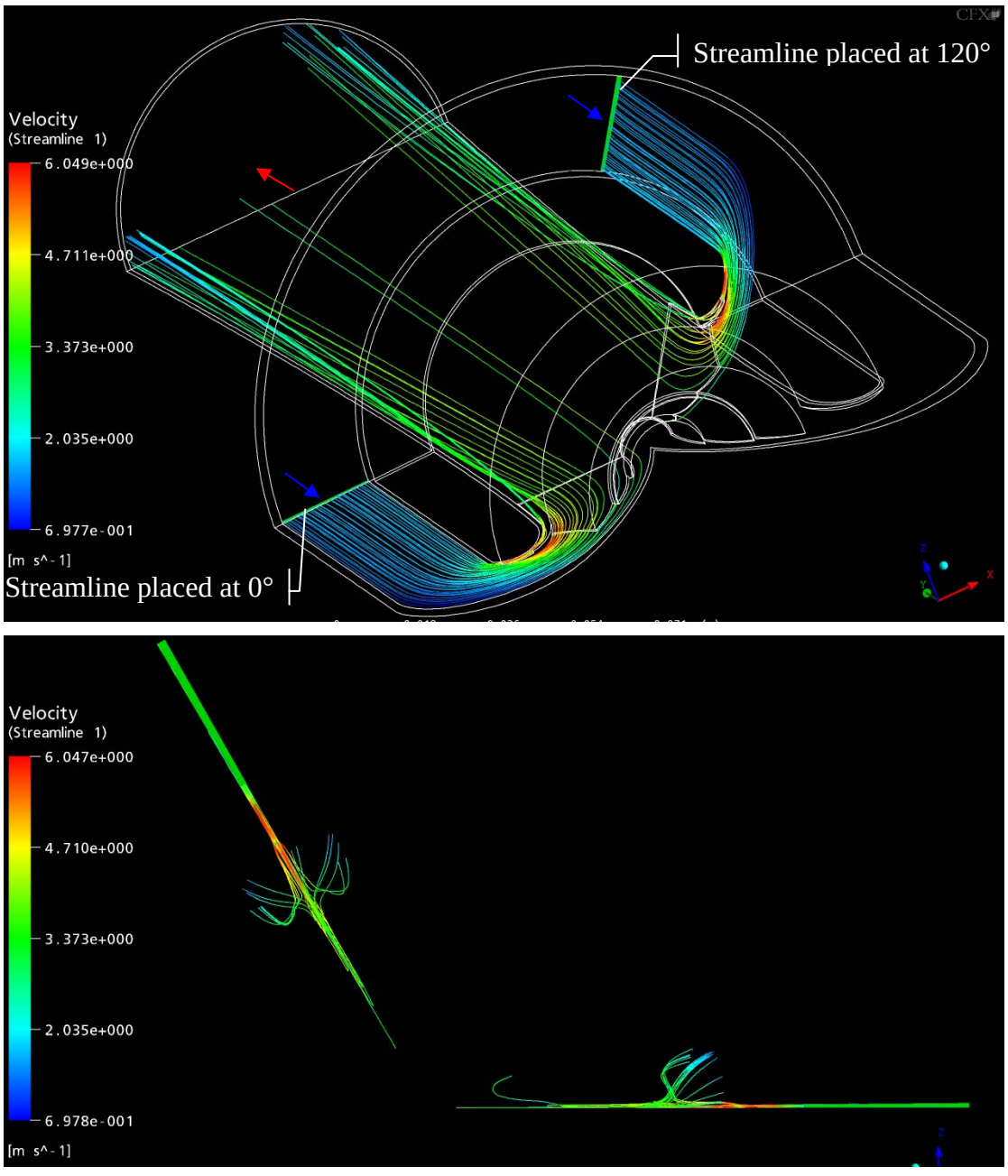

Figure 6-4. Detail of streamlines surrounding the vane supports located at 0° and 120° viewed in perspective (top) and from the inlet (bottom)

The streamlines intersect the support and –as expected- flow around the supports creating a local boundary layer. There is no vortex in the wake of the support however, and the zone of influence remains limited. In particular the flow on the inner

guide tube wall appears to be more perturbed than at the centre of the exiting outflow where the proton beam deposits most of its heat.

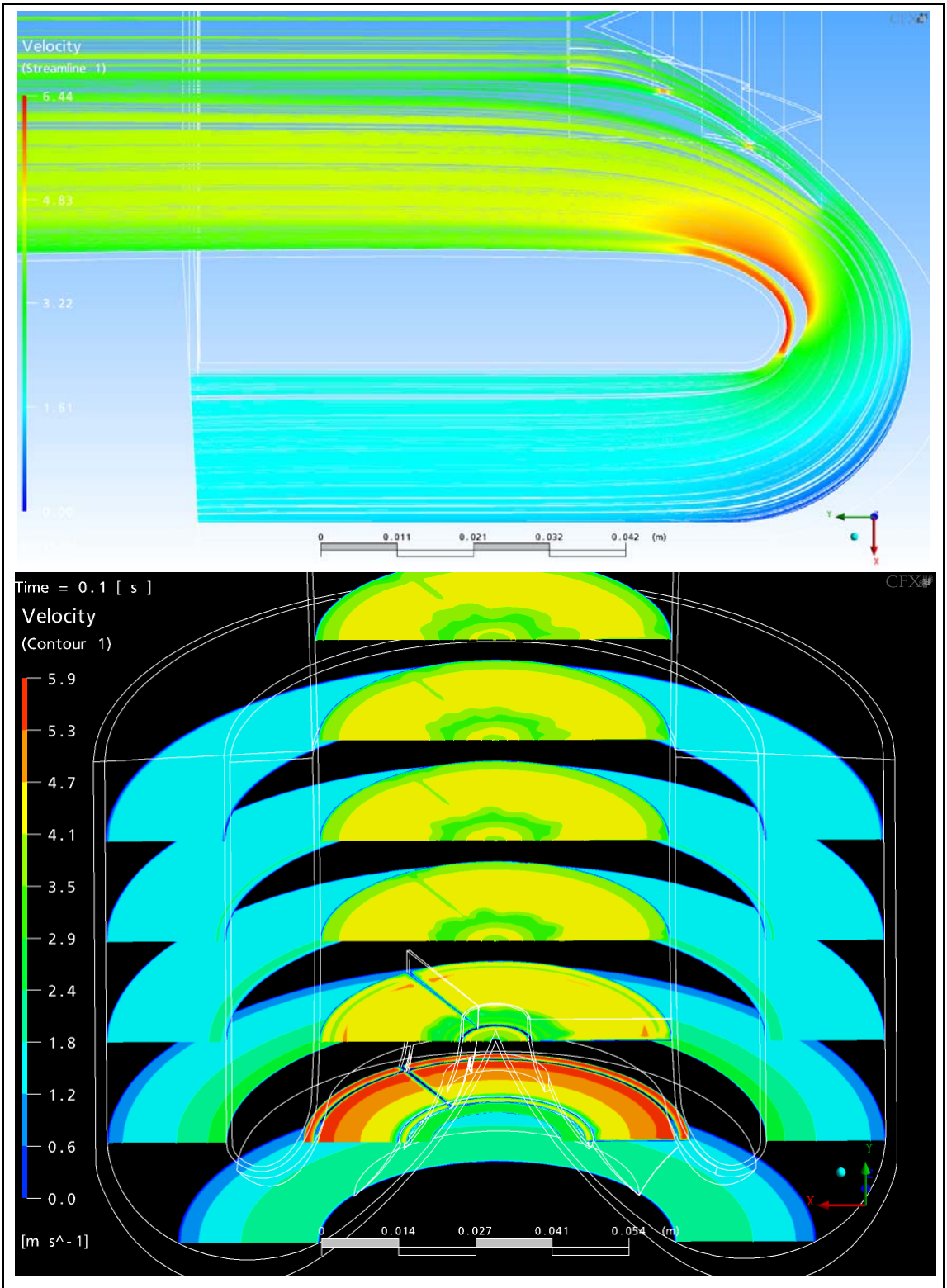

Figure 6-5. Detail of streamlines surrounding the vanes (top) and section view of velocity magnitude down the outlet channel (bottom)

The distribution of velocities in the inner channel in Figure 6-5 shows the increase in velocity around the vanes, particularly where the radius of turn is tightest, i.e. close to the guide tube fore end. The attachment of the flow to the window surface

due to the vanes is visible, the perturbation introduced by the vanes supports spaced out at 120° is also apparent.

The case where the beam is centred shows there are neither instability in the flow, nor perturbation introduced by the supports.

6.1.3 Beam off-centre by 5 mm

The case where the beam is off-centre must be evaluated as the stability of the 4[MW] proton beam is at present unknown. Based on prior experience it would appear that the beam may wander off course by no more than a few millimetres, and therefore 5 [mm] may regarded as a worst case.

It should be emphasized that the calculation considers the beam to be *static*, positioned at a point 5 [mm] off-centre along the symmetry axis. The velocity at which the beam may be displaced from the window centre to the off-axis position is not considered in this calculation. This parameter is unknown at this stage and yet it does have an influence, particularly on the stresses. Obviously in order to keep stresses as low as possible, any off-axis movement of the beam should be as slow as possible.

The first observation with regards to the off-axis beam calculation results is that the effect of buoyancy is indeed represented in the CFD model as may be seen in Figure 6-6 below.

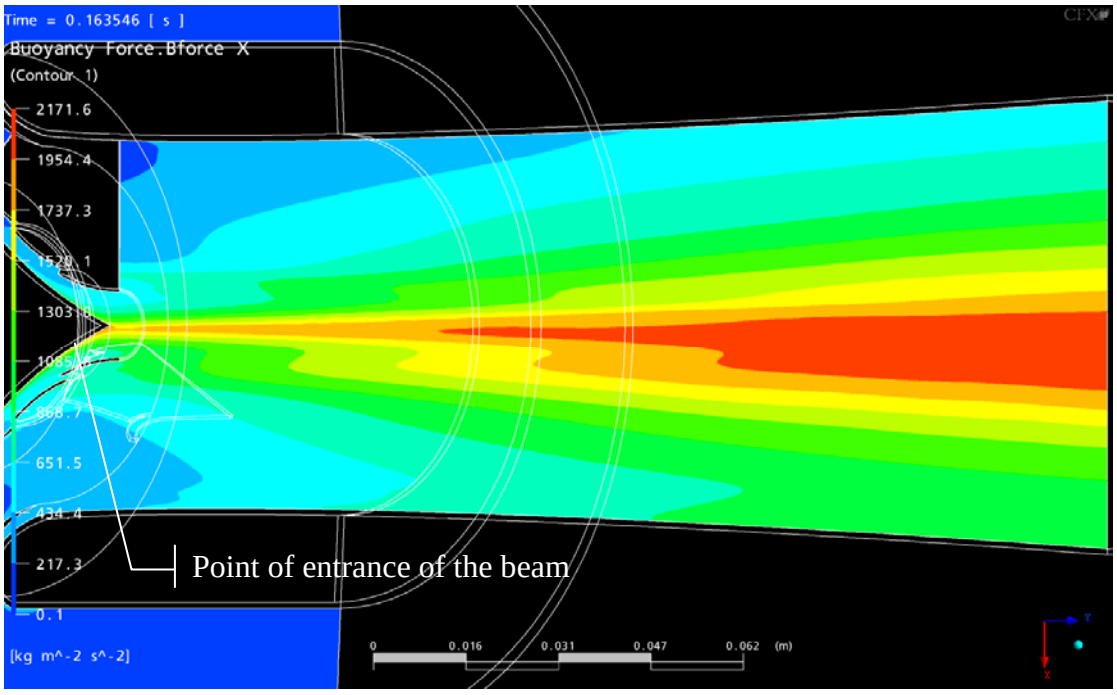

Figure 6-6. Buoyancy force in the LM with an off-axis beam

The effect of the off-axis beam on the temperature in the window is immediately apparent. There is a clear shift along the symmetry plane in the peak temperature of the window towards the off-axis position of the beam, as shown in Figure 6-7.

The magnitude of the temperature in the window and overall structure does not change however, compared to the on-axis case.

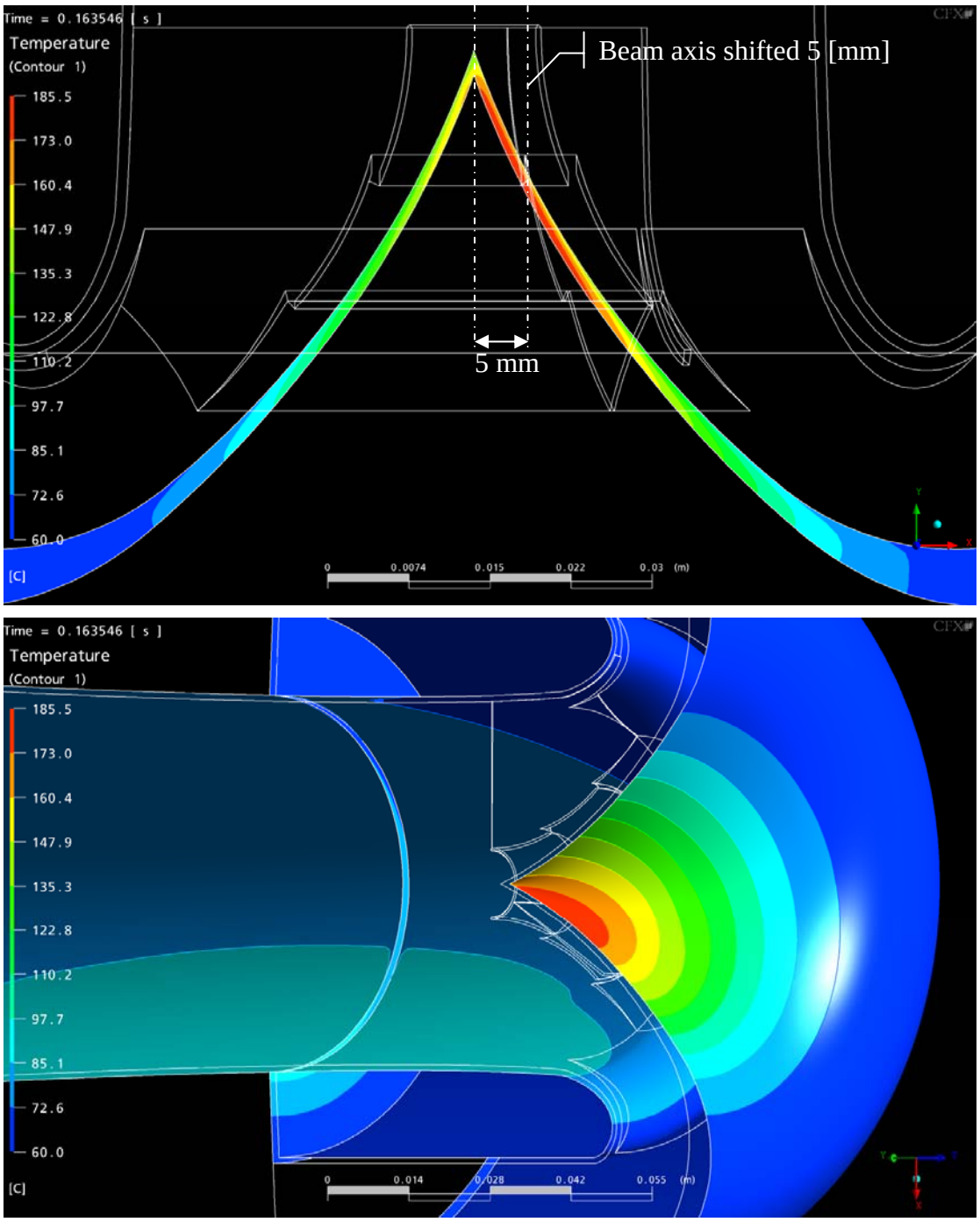

Figure 6-7. Detail of temperature distribution near point of entrance of the off-axis proton beam.

The streamlines are also of interest as the run is transient, and hence instabilities in the flow resulting from the off-axis position will show up. A section cut of the streamlines shown in Figure 6-8 indicates no serious perturbation from the off-axis position of the beam. The velocity contours in planes at right angle to the outlet flow is shown in the lower portion of Figure 6-8 and shows some slight disturbance of the flow pattern compared to a similar view taken with the beam on centre (Figure 6-5). This shift in the velocity field is due to a change in the buoyancy effect cause by shifting the beam. However the effect is not great as the stream wise velocity is far higher than the buoyancy-induced velocity component.

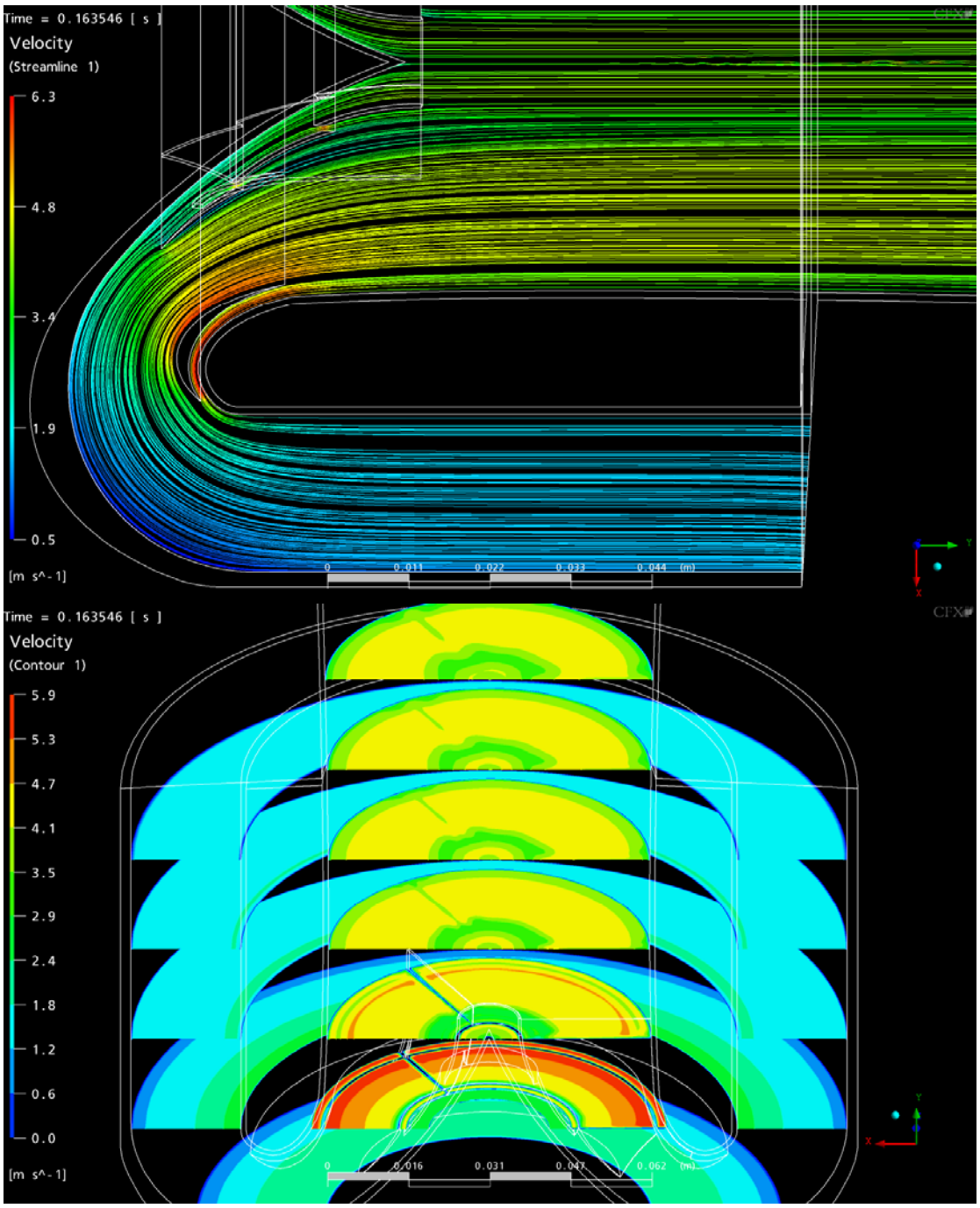

Figure 6-8. Detail of streamlines surrounding the vanes (top) and section view of velocity magnitude down the outlet channel (bottom)

7 Conclusion

A design has been proposed for the Eurisol converter target which is deemed relatively simple to manufacture as most steps do not resort to expensive manufacturing techniques or exotic materials. Undoubtedly the relatively thin window (0.8 mm currently) is a challenge; however there is an alternative design with a thicker window if a wider beam is selected.

The proposed design of the Eurisol target has been reviewed and checked for matters related to thermal, hydraulic performance and structural integrity. The analysis conducted thus far has shown that the design is able to fulfil the requirements set on the converter target.

Further analysis is needed to cover accident cases in particular. However the analysis of the off-centre beam shows that the target is able to withstand such imbalances with relative ease, such that no major problem is to be expected from a more detailed analysis, which will nevertheless be required for a full-blown production converter target.